



HAL
open science

The rostral ventromedial medulla control of cutaneous vasomotion of paws and tail in the rat: implication for pain studies

Nabil El Bitar, Bernard Pollin, Gan Huang, André Mouraux, Daniel Le Bars

► To cite this version:

Nabil El Bitar, Bernard Pollin, Gan Huang, André Mouraux, Daniel Le Bars. The rostral ventromedial medulla control of cutaneous vasomotion of paws and tail in the rat: implication for pain studies. *Journal of Neurophysiology*, 2016, 115 (2), pp.773-789. 10.1152/jn.00695.2015 . hal-01293011

HAL Id: hal-01293011

<https://hal.sorbonne-universite.fr/hal-01293011>

Submitted on 24 Mar 2016

HAL is a multi-disciplinary open access archive for the deposit and dissemination of scientific research documents, whether they are published or not. The documents may come from teaching and research institutions in France or abroad, or from public or private research centers.

L'archive ouverte pluridisciplinaire **HAL**, est destinée au dépôt et à la diffusion de documents scientifiques de niveau recherche, publiés ou non, émanant des établissements d'enseignement et de recherche français ou étrangers, des laboratoires publics ou privés.

1
2
3
4 **The rostral ventro-medial medulla (RVM) control of**
5 **cutaneous vasomotion of paws and tail in the rat. Implication for pain studies.**
6
7

8 Nabil El Bitar^{1,2,*}, Bernard Pollin^{1,2*}, Gan Huang³, André Mouraux³, Daniel Le Bars^{1,2,†}
9

10 *This paper is dedicated to our colleague and friend Bernard Pollin, who passed away while our work was*
11 *under redaction and whose contributions to this work were invaluable.*
12
13
14
15

16 1 Sorbonne Universités, Université Pierre et Marie Curie, Faculté de Médecine Paris, France.

17 2 Neurosciences Paris-Seine, Institut National de la Santé et de la Recherche Médicale UMRS-1130, Centre
18 National de la Recherche Scientifique UMR-8246, Paris, France.

19 3 Institute of Neuroscience, Université Catholique de Louvain, Brussels, Belgium

20 * These authors contributed equally to this work.

21 † To whom correspondence should be addressed. E-mail: daniel.le_bars@upmc.fr
22
23
24
25

26 **Number of pages:** 44

27 **Number of figures and tables:** 10 figures, 3 tables

28 **Number of words:** Abstract, 249; Introduction, 781; Discussion, 3438.

29 **Supplemental material:** 1 video
30

31 **Running head:** RVM control of cutaneous vasomotion
32

33 **Key words:** rat, thermoregulation, ambient temperature, skin temperature, environmental impact, blood
34 pressure, heart rate, infrared camera, rostral ventro-medial medulla, RVM, rostral Medullary Raphe, rMR.
35

36 **ABSTRACT**

37 Thermal neutrality in rodents is achieved by large cyclic variations of the sympathetic drive of the
38 vasomotion of the tail and paws, the most widely used target organs in current acute or chronic animal
39 models of pain. Given the pivotal functional role of rostral ventro-medial medulla (RVM) in nociception and
40 rostral Medullary Raphe (rMR) in thermoregulation, two largely overlapping brain regions, we aimed at
41 circumscribing the brainstem regions that are the source of premotor afferents to sympathetic preganglionic
42 neurons that control the vasomotor tone of the tail and hind-paws. A thermometric infrared camera recorded
43 indirectly the vasomotor tone of the tail and hind-paws. During the control period, the rat was maintained in
44 vasoconstriction by preserving a stable, homogeneous and constant surrounding temperature, slightly below
45 the core temperature. The functional blockade of the RVM/rMR by the GABA_A receptor agonist muscimol
46 (0.5 nmol, 50 nl) elicited an extensive increase of the temperature of the paws and tail, associated to slight
47 decrease of blood pressure and heart rate. Both the increased heat loss through vasodilatation and the
48 decrease heart-induced heat production elicited a remarkable reduction of the central temperature. The
49 effective zones were circumscribed to the parts of the RVM/rMR facing the facial nucleus. They match very
50 exactly the brain regions often described as specifically devoted to the control of nociception. Our data
51 support and urge on the highest cautiousness regarding the interpretation of results aimed at studying the
52 effects of any pharmacological manipulations of RVM/rMR with the usual tests of pain.

53

54 **INTRODUCTION**

55 Numerous studies have explored the descending systems that control the spinal transmission of
56 nociceptive messages, notably through the Rostral Ventromedial Medulla (RVM) in the brainstem. The
57 RVM includes the nucleus raphe magnus and the neighboring part of the reticular formation, which extends
58 under the gigantocellular reticular nucleus (Fields et al. 2006). Two main categories of neurons, so-called
59 "on-" and "off-" cells, were highlighted that: (1) exhibit irregular spontaneous activities in opposition of
60 phase (Barbaro et al. 1989) and (2) are activated and inhibited by nociceptive stimuli, respectively (Fields et
61 al. 1983; Vanegas et al. 1984). These two neuronal types were proposed to belong to a double spino-bulbo-
62 spinal positive feedback loop that facilitates the spinal transmission of nociceptive messages, either directly
63 or through a mechanism of disinhibition, the "on-" and "off-" cells being supposed to produce an excitatory
64 and an inhibitory drive on the spinal neurons, respectively.

65 However, RVM neurons could play a much less specific role than that of a descending pathway
66 modulating nociception at spinal level (Le Bars et al. 2001; Lefler et al. 2008; Lovick 1997; Mason 2001;
67 2005a; 2005b; 2006; 2011; 2012; Thurston and Helton 1996; Thurston and Randich 1992; 1995). For
68 example, we described recently the probable involvement of "on-" and "off-" cells in autonomic regulation,
69 notably thermoregulation (El Bitar et al. 2014b).

70 On the basis of three animal models used in thermoregulation studies, namely the tail of the rat, the
71 ear of the rabbit and the interscapular brown adipose tissue (BAT) of the rat, it became apparent that neurons
72 in the midline region of the ventral medulla play a critical role in responding to cold (Blessing et al. 1999;
73 McAllen et al. 2010, Morrison 1999, 2011; Morrison et al. 1999, 2008, 2012; Nakamura 2011; Nakamura
74 and Morrison 2008, 2011; Rathner et al. 2001; Rathner and McAllen 1999; Tanaka et al. 2002). Broadly,
75 cooling the animal results in (1) reduced heat loss through increased skin vasoconstriction of the ear in the
76 rabbit or the tail in the rat and (2) increased heat production by BAT in the rat. These phenomena are
77 triggered by activation of sympathetic preganglionic neurons in the spinal intermediolateral cell column,
78 themselves under the control of premotor neurons located in the rostral Medullary Raphe (rMR), a region
79 immediately rostral to the rostral pole of the inferior olivary complex, that includes the raphe pallidus, the
80 raphe magnus and the laterally extending parapyramidal nucleus (Blessing 2003; McAllen et al. 2010;
81 Morrison 2011; Nakamura 2011; Nakamura and Morrison 2008, 2011), where the expression of Fos
82 immunoreactivity is increased following cold exposure (Bonaz and Taché 1994; Cano et al. 2003; Morrison
83 et al. 1999; Nakamura et al., 2004).

84 Yet a possible discrepancy was noted. Studies focusing on the descending systems postulated to
85 control nociception emphasize a region which includes the nucleus raphe magnus and the gigantocellular
86 reticular nucleus pars alpha, mainly at the level of the facial nucleus (e.g. Brink et al. 2006; Carlson et al.
87 2007; Fields et al. 1995; Heinricher and Kaplan 1991; Heinricher and Tortorici 1994; Kaplan and Fields
88 1991; Morgan and Fields, 1994; Neubert et al. 2004; Vanegas et al. 1984; Thurston and Helton, 1996;
89 Thurston and Randich, 1995; Xu et al. 2007), while studies focusing on thermoregulation emphasize a
90 slightly more caudal region including the raphe pallidus (e.g. Blessing and Nalivaiko, 2001; Cao and
91 Morrison 2003; Cao et al. 2004, 2010; Cerri et al. 2010; Fan et al. 2007; Madden and Morrison 2003, 2005;

92 Morrison 1999, 2003, 2004; Morrison et al. 1999, 2000; Nakamura and Morrison 2007, 2011; Nakamura et
 93 al. 2004; Ootsuka and McAllen 2005; Rathner et al. 2001, 2008; Salo et al. 2009; Tanaka et al. 2002, 2007;
 94 Yoshida et al. 2003).

95 The aim of the present study was therefore to map exactly the brainstem regions that contain the
 96 premotor sympathetic neurons controlling the vasomotor tone of the tail and hind-paws of the rat, and to
 97 compare these locations with that of nociception-related brainstem areas. This choice was made specifically
 98 because many behavioral models of pain/nociception are based on the assessment of the response of a rodent
 99 to a thermal stimulus applied to the tail or a hind-paw (reviewed in Le Bars et al. 2001, 2009).

100 Specifically, we measured in 160 adult male Sprague-Dawley rats, the dynamic changes in
 101 vasomotor tone induced by microinjections of muscimol within these regions. During the injection, the rats
 102 were maintained in a stable state of tail and hind-paw vasoconstriction. Microinjection of muscimol within
 103 the RVM/rMR was expected to elicit vasodilation of the tail and hind-paw. When a vasomotor response was
 104 present, the latency at which vasodilation occurred was used as an index of the distance between the
 105 injection site and the structure generating the response.

106

107 GLOSSARY

108

7	<i>Facial nucleus</i>
α	<i>Slope of the squared temperature variation elicited by a radiant heat source ($^{\circ}\text{C}^2/\text{s}$)</i>
BAT	<i>Brown adipose tissue</i>
bpm	<i>Beats per minute</i>
ΔT_{skin}	<i>Amplitude of the skin temperature variation ($^{\circ}\text{C}$)</i>
Δt	<i>Duration of the ascending phases of vasodilatation ($= t_{\text{max}} - t_{\text{min}}$)</i>
ETCO ₂	<i>End-tidal CO₂</i>
GiA	<i>Gigantocellular reticular nucleus pars alpha</i>
HLI	<i>Heat Loss Index</i>
HR	<i>Mean heart rate (bpm)</i>
LPGi	<i>lateral paragigantocellular nucleus.</i>
MAP	<i>Mean arterial blood pressure (mmHg)</i>
ml	<i>Medial lemniscus</i>
paw-contra	<i>Mid-plantar area on the hind-paw, contralateral to the injection site</i>
paw-ipsi	<i>Mid-plantar area on the hind-paw, ipsilateral to the injection site</i>
PPy	<i>Parapyramidal nucleus</i>
py	<i>Pyramidal tract</i>
RMg	<i>Raphe magnus nucleus</i>
rMR	<i>Rostral Medullary Raphe</i>
RPa	<i>Raphe pallidus nucleus</i>

<i>ROI</i>	<i>Region of interest</i>
<i>RVM</i>	<i>Rostral Ventro-medial Medulla</i>
<i>RVM/rMR</i>	<i>Combination of RVM and rMR</i>
<i>s</i>	<i>spread of the sigmoid curve</i>
t_{min}	<i>Beginning time of the ascending phase of vasodilatation (min)</i>
t_{max}	<i>End time of the ascending phase of vasodilatation (min)</i>
t_x	<i>Abscissa of the inflection point of Boltzmann sigmoid (min)</i>
T_{adj}	<i>Sigmoid Boltzmann curve adjusted to the recorded temperature</i>
T_{amb}	<i>Ambient temperature (°C)</i>
T_{core}	<i>Core body temperature (°C)</i>
T_{max}	<i>Adjusted maximal skin temperature at the end of the process of vasodilatation (°C)</i>
T_{min}	<i>Adjusted skin temperature during the control period (°C)</i>
$T_{paw-contra}$	<i>Temperature of the plantar aspect of the hind-paw, contralateral to the injection site (°C)</i>
$T_{paw-ipsi}$	<i>Temperature of the plantar aspect of the hind-paw, ipsilateral to the injection site (°C)</i>
T_{skin}	<i>Temperature of the skin (°C)</i>
$T_{tail-dist}$	<i>Temperature of the distal part of the tail (°C)</i>
$T_{tail-mid}$	<i>Temperature of the mid part of the tail (°C)</i>
$T_{tail-prox}$	<i>Temperature of the proximal part of the tail (°C)</i>
T_x	<i>Ordinate of the inflection point of Boltzmann sigmoid (°C)</i>
<i>tail-dist</i>	<i>Distal area of the tail, located at 3 cm from the tip</i>
<i>tail-mid</i>	<i>Intermediate area of the tail, located at mid-tail</i>
<i>tail-prox</i>	<i>Proximal area of the tail, located at 3 cm from the root of the tail</i>
<i>TFL</i>	<i>Tail-flick latency (s)</i>
$T_{tail-mid}$	<i>Temperature of the mid part of the tail (°C)</i>
$T_{tail-prox}$	<i>Temperature of the proximal part of the tail (°C)</i>
T_{warm}	<i>Warming temperature (°C)</i>
<i>x</i>	<i>latero-lateral coordinate with reference to the interaural line</i>
<i>y</i>	<i>ventro-dorsal coordinate with reference to the interaural line</i>
<i>z</i>	<i>rostro-caudal coordinate with reference to the interaural line</i>

110 **METHODS**

111

112 *Ethic statement*

113 Animal experiments were performed with permission of the Board of the Veterinarian Services of
114 the French Ministry of Agriculture (permit number 75-151) in accordance with the National Institute of
115 Health's "Guide for the care and use of Laboratory animals", the European Communities Council Directive
116 86/609/EEC regulating animal research, and the ethics committee of the International Association for the
117 Study of Pain (Covino et al. 1980; Zimmermann 1983). The Committee of Ethics for the Animal Experiment
118 of our Institution approved the procedures.

119

120 *Animals*

121 Experiments were performed on 160 adult male Sprague-Dawley rats (Janvier Labs, Saint-Berthevin,
122 France) weighing 320-370 g. They were housed in groups of 3-4 per cage, allowed free access to food and
123 water with a 12 h alternating light-dark cycle, and acclimatized to the laboratory for at least one week before
124 the experiment. The experiments were conducted between 9 AM and 5 PM.

125

126 *Experimental procedure*

127 The animals were deeply anesthetized with 2.5% halothane in 100% oxygen. A tracheal cannula was
128 inserted and the ventilation was controlled mechanically with an open circuit respirator equipped with a
129 scavenging system, at a rate of 50 breaths/min. The tidal volume was adjusted to maintain a normal end-tidal
130 CO₂ (ETCO₂). The expiratory halothane level and ETCO₂ were assessed with a capnometer (Capnomac II,
131 Datex Instruments, Helsinki, Finland), recorded each ten seconds and under control of alarms throughout the
132 experiment. The mean arterial blood pressure (MAP) and heart rate (HR) were monitored continuously via a
133 catheter inserted into the common carotid artery and connected to a computer via a transducer. MAP and HR
134 were calculated and recorded using the NOTOCORD[®] blood pressure analyzer system.

135 The body of the animal was wrapped up in a water-warming pad connected to an extra-capacity
136 water circulator (TP 220-Kent, scientific corporation) sparing the head, the paws and the tail. The heating
137 blanket was covered with an isothermic metalized polyester film ("survival blanket") to stabilize the space
138 temperature around the body. A two channel OMEGA[®] HH506RA digital thermometer and two VIP-T-
139 CT25515 Probes (0.1°C resolution) were used to measure the core temperature T_{core} (throughout a rectal
140 probe inserted 10 cm) and the heating temperature T_{warm} (probe placed between the warming pad and the
141 trunk of the rat). We adjusted T_{warm} in order to maintain (1) T_{core} stable within normal physiological values
142 and (2) the tail and hind-paws in vasoconstriction.

143 The rat was mounted on a Horsley-Clarke stereotaxic frame. 0.5 ml of xylocaine 2% was injected
144 subcutaneously in the scalp, followed by a 2-cm midline incision. After trepanation, a small incision of the
145 dura-mater was made to introduce the tip of a microinjection glass needle.

146 After surgery, halothane was decreased to 0.8-0.9% with oxygen being kept at 100%, the tidal
147 volume was adjusted to keep the ETCO₂ around 3.5% and at least 30-min were waited before starting the

148 experimental procedure. After 15-min of control period in steady vasoconstriction, 57 ng (50 nl) muscimol
149 were injected in the RVM/rMR (target zone between -0.8 and -3.3 rostral to inter-aural line) over 60-
150 seconds. Since RVM and rMR largely overlap, we will refer to “RVM/rMR” for brain regions that include
151 the raphe pallidus, raphe magnus, parapyramidal nucleus and the reticular formation that extends under the
152 gigantocellular reticular nucleus (Mason 2001, 2005a, 2005b, 2006, 2011). Control experiments were
153 conducted with the same procedure, except that muscimol was injected outside the RVM/rMR.

154

155 ***Experimental conditions***

156 The experiments were made in anesthetized rat with unremitting halothane level [0.85 (0.83-
157 0.86)%], while ventilation was controlled in order to achieve a stable and normal acid-base equilibrium
158 during the control period $ETCO_2 = 3.65$ (3.57-3.73)%. The mean room temperature T_{amb} was stable at 24.2
159 (24.1-24.4)°C. The paws and tail of the rat were maintained in vasoconstriction during the control period by
160 preserving a stable, homogeneous and constant surrounding temperature [$T_{warm} = 37.4$ (37.2-37.5)°C], \approx
161 0.3°C below T_{core} [37.7 (37.6-37.8)°C], and kept constant till the end of the experiment. In the control period,
162 MAP and HR were 83.9 (77.4-90.4) mmHg and 321 (309-332) bpm, respectively.

163

164 ***Muscimol preparation***

165 We prepared muscimol solution in a concentration of 0.01 nmol/nl, added pontamine sky blue to
166 identify the site of injection, fractioned the solution in 2 μ l aliquots for single use and preserved them at -
167 20°C. Muscimol produces a rapid and persistent hyperpolarization of neurons (Hikosaka and Wurtz 1985;
168 Martin and Ghez 1999) based on its high affinity and selectivity for the GABA_A receptor (Beaumont et al.
169 1978; Enna and Snyder 1975; Gallagher et al. 1983; Krogsgaard-Larsen et al. 1977; Nicholson et al. 1979).
170 The day of the experiment, we filled the circuit of the glass needle with paraffin to wash out air bubbles,
171 aspirated 0.5 μ l of muscimol solution at the tip of the needle using a 1- μ l Hamilton syringe and introduced
172 the needle in the brain at the end of the surgery..

173

174 ***Thermographic recordings***

175 Under stable environmental temperature, skin temperature is a reliable indicator of skin blood flow
176 variations (El Bitar et al. 2014a, Hertzman 1953). Heat transmission from deeper tissue to the skin occurs by
177 conduction and vascular convection, and then heat dissipation to the environment through conduction,
178 convection, evaporation and radiation processes. The spatial and temporal evolution of the skin temperature
179 at the level of the tail and paws was monitored using a JADE MWIR (3-5 μ m optical bandpass) camera
180 (CEDIP Infrared Systems, Croissy-Beaubourg, France) with a 500 μ s integration time, which supplied
181 images of 320x240 pixels at 1 Hz with a sensitivity of 0.02°C at 25°C. The camera was placed 1.5 m upright
182 to the scene and was controlled by the software Cirrus[®] (CEDIP Infrared Systems, Croissy-Beaubourg,
183 France). It was calibrated by means of a black body as previously described (Benoist et al. 2008).

184 Recently, we verified the highly significant positive linear correlation between skin temperature and
185 skin blood flow measured by a laser-Doppler probe. The mean time lag between vasodilatation and skin

186 temperature increase was estimated at around half a minute (El Bitar et al. 2014a). Such an approach based
 187 on thermal imaging has the advantage of giving accurate measures of temperature at both temporal and
 188 spatial levels.

189 Analysis of the thermographic films was made using the software Altair[®] (CEDIP Infrared
 190 Systems, Croissy-Beaubourg, France). Ten regions of interest (ROI) were defined in the recorded scene,
 191 each comprising 10 pixels. Five ROIs were located on the dorsal aspect of the tail. A proximal ROI (tail-
 192 prox) was placed 3 cm from the root of the tail, an intermediate ROI (tail-mid) was placed at the middle of
 193 the tail, and a distal ROI (tail-distal) was placed 3 cm from the tip of the tail. The remaining two zones were
 194 distributed equidistantly between tail-prox and tail-mid and tail-mid and tail-dist. Two additional ROIs were
 195 located on the plantar aspect of each hind paw; their final designation was defined respective to the side of
 196 muscimol microinjection, ipsilateral (paw-ipsi) or contralateral (paw-contra), as determined following
 197 histological controls. Finally, a ROI was located over a piece of wood placed in the scene to monitor the
 198 ambient temperature (T_{ambient}). For each time point, the mean of the ten pixels defining each ROI was
 199 computed to obtain one single temperature time course for each ROI ($T_{\text{tail-prox}}$, $T_{\text{tail-mid}}$, $T_{\text{tail-dist}}$, $T_{\text{paw-left}}$, $T_{\text{paw-}}$
 200 right and T_{ambient}).

201

202 *Histological identification of microinjection sites*

203 At the conclusion of the experiment, the rat was deeply anesthetized with 3% halothane and the brain
 204 was perfused through the heart with 0.9% NaCl, followed by 10% formaldehyde and removed. The brain
 205 was frozen, cut in serial 100- μm thick sections and Nissl-stained with cresyl violet or carmin. Sites of
 206 microinjections were determined from microscopic visualization of the serial sections and reported on
 207 schemas of frontal sections of the brain (Paxinos and Watson 2005). Coordinates were then expressed
 208 relative to the interaural line: x-axis = latero-lateral; y-axis = ventro-dorsal; z-axis = rostro-caudal. The
 209 center of injection was easy to delimit. On average ~ 1 hour post injection, the overall rostro-caudal diffusion
 210 of pontamine blue was 1.1 mm (1.0-1.2 mm), and two times larger than diffusion in the coronal plane.

211

212 *Assessing the dynamic effects of muscimol on skin temperature*

213 The skin temperature evolution following muscimol microinjection matched a sigmoid curve. The
 214 curves were adjusted to a Boltzmann sigmoid according to the equation $T_{\text{adj}} = T_{\text{min}} + \Delta T_{\text{skin}} / \{1 + \exp[-(t -$
 215 $t_x)/s]\}$, using the SigmaPlot[®] software. Time $t = 0$ corresponded to the end of the microinjection (Fig. 1A).
 216 The following parameters were fitted to the data: T_{min} (adjusted skin temperature during the control period),
 217 T_{max} (adjusted maximal skin temperature at the end of the process), $\Delta T_{\text{skin}} = T_{\text{max}} - T_{\text{min}}$ (amplitude of the skin
 218 temperature variation), t_x (abscissa of the inflection point of the sigmoid), T_x (ordinate of the inflection point
 219 of the sigmoid), s = spread of the sigmoid curve. These parameters were calculated for the proximal and
 220 distal parts of the tail, and for each hind-paw. The regression coefficients R^2 of the adjusted curves were
 221 always highly significant (> 0.98).

222 The regulation of the laboratory air-conditioning system was a source of change of ambient
 223 temperature in the $\sim 0.5^\circ\text{C}$ range. This represented $\sim 10\%$ of the magnitude of the ascending phase of

224 muscimol-induced increases in skin temperature at the hind-paws and distal part of the tail and ~15% of the
 225 increases in skin temperature at the proximal tail. Therefore, the beginning (t_{\min}) of the ascending phase of
 226 vasodilatation at the hind-paws and distal part of the tail was calculated by considering the 10% percentile of
 227 ΔT_{skin} : $t_{\min} = t_x - S \cdot \text{Ln}(1/0.1-1)$ (Fig. 1B). A slightly different cutoff (15%) was chosen to estimate the onset
 228 of vasodilatation at the proximal part of the tail, because of the slower evolution of the process at that location.
 229 The end (t_{\max}) of the ascending phase of vasodilatation was calculated by considering the 90% percentiles of
 230 ΔT_{skin} : $t_{\max} = t_x - S \cdot \text{Ln}(1/0.9-1)$.

231 Then, the latency of the vasomotor reactions were divided into three groups according to the
 232 distribution of the beginning time t_{\min} of the ascending phase of vasodilatation: $t_{\min} < 7.5$ min, $7.5 < t_{\min} < 15$
 233 min and $t_{\min} > 15$ min. This categorization was justified by the clear bimodal distribution of t_{\min} , centered on
 234 3-5 and 10-12 min, respectively (Fig. 1C). Beyond 15 min, the distribution of t_{\min} was flat, and the observed
 235 effects if any were interpreted as resulting from uncontrolled diffusion of muscimol (Edeline et al. 2002).
 236 Together with a small volume of injection (50 nl) and a large number of negative sites of injection, this
 237 approach provided an acute delineation of the structures controlling sympathetic cutaneous vasoconstrictor
 238 activity.

239

240 *Three-dimensional mapping of response latencies*

241 The large number of microinjection sites provided the opportunity of building a three-dimensional
 242 mapping of response latencies as a function of injection site, using interpolation. The interpolation was
 243 performed by computing an average of the responses obtained at all injection sites, weighted by the distance
 244 between the interpolated voxel and each injection site. This ensured that the interpolated values were most
 245 dependent on the responses of the nearest injection sites. In addition, because of the non-homogeneous
 246 sampling of the interpolated volume, a mask was used to exclude voxels that were not close to at least one
 247 injection point.

248 For each measurement location (left paw, right paw, proximal tail, distal tail), a 3D volume
 249 representing response latencies as a function of injection site was obtained using interpolation. The responses
 250 obtained from the left and right paw were merged, by expressing the location of the injection site as
 251 ipsilateral (positive x-axis) vs. contralateral (negative x-axis) relative to the paw. The interpolated 3D
 252 volume extended from -2 mm to +2 mm along the x-axis, -1.5 mm to +1 mm along the y axis, and -1 mm to
 253 +3.5 mm along the z-axis (200 points along each dimension). For each voxel of the volume, an interpolated
 254 latency was obtained by computing a weighted average of all latency values:

$$\text{latency}(x, y, z) = \frac{\sum w_i \text{latency}_i}{N}$$

255

256 The weight assigned for each latency value (w_i) was determined by the distance between the voxel
 257 (x, y, z) and the injection site (x_i, y_i, z_i):

$$w_i = \frac{1}{(\sqrt{(x_i - x)^2 + (y_i - y)^2 + (z_i - z)^2})^6}$$

258 This weight is inversely proportional to the sixth power of the distance. This ensured that at any
 259 given location of the interpolated volume, interpolated latencies were more dependent on the latencies of the
 260 nearest injection site. Because the 3D volume was not homogeneously sampled (i.e. injection sites were
 261 clustered in some regions of the volume), a mask was used to exclude voxels, which were not located at a
 262 distance < 0.5 mm of at least one injection point. Finally, because injection at a large amount of sites did not
 263 elicit any response, a second mask was computed to distinguish voxels located in regions where injection
 264 elicited a response from voxels located in regions where injection did not elicit a response after 55 min of
 265 recording. After assigning a latency of 55 min to these trials, the second mask was computed by taking all
 266 voxels of the interpolated volume having interpolated latencies above an arbitrary interpolated latency value
 267 of 53.5 min.

268

269 ***Heat loss Index***

270 The skin is an interface between core temperature (T_{core}) and ambient temperature, (T_{amb}) acting as a
 271 radiator. In addition to active changes secondary to vasomotor tone of skin vessels, the temperature T of the
 272 skin can be affected passively by either T_{amb} or T_{core} . To cancel out these passive changes, we computed the
 273 Heat Loss Index (HLI) = $(T_{\text{skin}} - T_{\text{amb}})/(T_{\text{core}} - T_{\text{amb}})$ as initially proposed by Székely (1986). The value of HLI
 274 can vary between 0 and 1, representing complete vasoconstriction ($T = T_{\text{amb}}$) and complete vasodilatation (T
 275 = T_{core}), respectively (Gordon et al. 2002; Romanovsky et al. 2002).

276

277 ***Analysis of vital signs***

278 To study the systemic effects of muscimol on MAP, HR, ETCO_2 and T_{core} with respect to the
 279 microinjection sites, we divided the experiments in three groups on the basis of the beginning time t_{min} of the
 280 ascending phase of vasodilatation. Group 1: (1) $t_{\text{min}} < 15$ min for all considered skin areas either on the tail or
 281 the paws. Group 2: $t_{\text{min}} < 15$ min for at least one but not all the areas considered on the tail or the hind-paws.
 282 Group 3: $t_{\text{min}} > 15$ min for all considered skin areas either on the tail or the paws. The mean of each variable
 283 during the control period was considered as the reference level, and the temporal evolution was calculated in
 284 terms of variation of this level, namely T_{core} ($\Delta^\circ\text{C}$), MAP (ΔmmHg), HR ($\Delta^\circ\text{C}$) and ETCO_2 ($\Delta\%$).

285

286 ***Data processing and statistical analyses***

287 The temporal evolution of the mean skin temperature, MAP and HR were synchronized and
 288 measured with a one-second-time resolution. The corresponding time courses were downsampled to a one-
 289 minute time resolution by averaging. Data were expressed as means (\pm confident interval 95%). The
 290 comparisons were done using the Mann Whitney U test and the Friedman repeated measures ANOVA on
 291 ranks test.

292

293 **RESULTS**

294

295 The paws and tail of the rat were successfully maintained in vasoconstriction during the control
 296 period by preserving a stable, homogeneous and constant surrounding temperature T_{warm} , adjusted to a few
 297 tenths degrees below T_{cor} , and by keeping this temperature constant throughout the experiment. Following a
 298 15-min period of control in steady vasoconstriction, muscimol (0.5 nmol, 50 nl) was injected over 60-
 299 seconds.

300 We will first describe in details a typical recording. Then the effects of muscimol will be detailed
 301 with reference to the injection sites determined post-mortem. Emphasis will be made on the comparison
 302 between hind-paws (ipsilateral vs. contralateral to the injection site). We seized the opportunity of the large
 303 number of microinjection sites to build three-dimensional mappings of response latencies as a function of
 304 injection site, using interpolation. Results will also be synthesized by taking into account concomitant
 305 variations of MAP, HR and T_{core} . Finally, the potential effect of muscimol on a widely used nociceptive test,
 306 the tail-flick test, will be assessed by using the present results to compute expected variations in tail-flick
 307 latency elicited by the effects of muscimol on both tail temperature and T_{core} .

308

309 ***A typical example of the effects of muscimol microinjection within the RVM/rMR***

310

311 An example of a thermographic film is provided as supporting information (Supporting video), from
 312 which a series of seven images recorded during 30-min are shown in figure 2A. These images correspond to
 313 a typical example of a microinjection centered to the RMg, as determined following histological examination
 314 (Fig. 2H). Figure 2B shows the temporal evolution of the temperature of (1) the hind-paws, ipsilateral (T_{paw-}
 315 $ipsi$) and contralateral (T_{paw-} $contra$) to the microinjection site, (2) five sites on the tail and (3) a small piece of
 316 wood, indicator of the ambient temperature (T_{amb}). Figure 2C shows the temporal evolution of the core
 317 temperature (T_{core}). During the control period, T_{amb} and T_{core} were stable while the hind-paws and tail were in
 318 vasoconstriction with skin temperatures slightly above T_{amb} . Following the injection of muscimol, a
 319 progressive increase of skin temperature is observed, starting at the ipsilateral paw (T_{paw-} $ipsi$: 4.9 min post-
 320 injection), followed by the proximal tail (T_{tail-} $prox$: 6.6 min), the distal tail (T_{tail-} $dist$: 11.6 min), and, finally, the
 321 contralateral paw (T_{paw-} $contra$: 12.6 min). The time courses of T_{paw-} $ipsi$ and T_{paw-} $contra$ were similar, increasing by
 322 8.2 and 7.4°C, within 7.7 and 8.0 min respectively, and remaining stable afterwards. The temporal evolution
 323 of the temperature of the tail was quite different, taking 26.6 min to achieve a 6.4°C increase for T_{tail-} $prox$ vs.
 324 21.2 min to achieve a 7.8°C increase for T_{tail-} $dist$. The intermediate parts of the tail showed a similar evolution
 325 whose parameters spread out between those of the extreme parts.

326 Shortly after vasodilatation of the ipsilateral hind-paw, one sees a decrease in core temperature (T_{core})
 327 (Fig. 2C) that was accentuated by the later vasodilatation of the tail and contralateral hind-paw. Overall, T_{core}
 328 was reduced by 0.8°C within the 30 min post-injection period despite the active warming that remained
 329 stable all over the experiment. The Heat Loss Indexes are shown in figure 2D for each site of T_{skin} skin
 330 recording.

331 MAP (Fig. 2E) and HR (Fig. 2F) were also affected by muscimol. Both parameters dropped and
 332 stabilized within 8 min, that is a few minutes earlier than the vasodilatation. At 30 min, the final MAP and
 333 HR were 36% and 20% less than during the control period, respectively. These variations were associated
 334 with a decrease of ETCO_2 (Fig. 2G).

335 From such an example, one can infer that microinjection of muscimol centered on the RMg is able to
 336 block the drive of the sympathetic control of vasomotion of the hind-paws and the tail, leading to an increase
 337 in their skin temperature and a subsequent decrease in T_{core} . The effects were dominant on the part of the
 338 body ipsilateral to the microinjection site. These variations were associated with a decrease in MAP, HR and
 339 ETCO_2 .

340

341 *Overall effect of muscimol microinjection within the RVM/rMR on the vasomotion of the hind-paws*

342

343 During the control period, both hind-paws were vasoconstricted at a stable skin temperature, close to
 344 the ambient temperature. The microinjection of muscimol in the RVM/rMR elicited an increase of the
 345 plantar skin temperature, indicating increasing blood flow. This reaction always started first in the ipsilateral
 346 hind-paw. Following adjustment of each individual curve to a sigmoid by a Boltzmann regression (see Fig.
 347 1AB), the experiments were divided in three groups on the basis of the distribution of the beginning (t_{min}) of
 348 the ascending phase of vasodilatation at the hind-paw ipsilateral to the microinjection site (Fig. 1C): group 1
 349 (acute onset group: $t_{\text{min}} < 7.5$ min); group 2 (intermediate onset group: $7.5 < t_{\text{min}} < 15$ min); group 3 (late
 350 onset or no response group: $t_{\text{min}} > 15$ min). The corresponding temporal evolutions of adjusted skin
 351 temperatures are shown in Figure 3 for the 3 groups. Regarding the two groups showing responses with acute
 352 or intermediate onset, the ipsilateral and contralateral curves were essentially parallel, but the response
 353 elicited in the latter was postponed by 11-12 minutes. The ascending phase of vasodilatation Δt was short
 354 lasting (in the 6-8 min range) and large (in the 7-8°C/min range), therefore steep (in the 1°C/min range). The
 355 corresponding numerical data are provided in table 1A.

356 Figure 4 shows the corresponding localization of the muscimol microinjection sites reported on the
 357 atlas of the rat brain by Paxinos and Watson (2005). For clarity of presentation, the data related to the hind-
 358 paws, ipsilateral and contralateral to the microinjection sites, are shown on the right and left parts of the
 359 figure, respectively. The black, grey and white circles represent microinjection sites related to experiments
 360 belonging to the first, second and third groups, respectively. Regarding the ipsilateral hind-paw, the most
 361 effective sites are located between planes -1.3 and -2.8 mm with reference to the inter-aural line, mainly in
 362 raphe pallidus, inner layer of raphe magnus and parapyramidal nucleus (Fig. 4B). These points are
 363 surrounded laterally and rostro-caudally by the second group (grey symbols), often localized in the outer
 364 layer of the raphe magnus. The non-reactive regions are outside these zones. The effects of microinjection on
 365 the contralateral hind-paw (Fig. 4A) were very much dependent on its proximity to the midline.
 366 Microinjections distant from the midline by less than 0.1 mm exhibited an acute onset effect, and those by
 367 less than 0.3 mm an intermediate onset effect.

368 We seized the opportunity of the large number of microinjection sites to build a three-dimensional
 369 mapping of response latencies as a function of injection site, using interpolation (Fig. 5). Since the effects
 370 were clearly lateralized, the responses obtained from the left and right paw were merged, by expressing the
 371 location of the injection site as ipsilateral (positive x-axis) vs. contralateral (negative x-axis) relative to the
 372 paw. The earliest responses latencies were observed between planes $z = -1.3$ and $z = -2.8$ mm both from the
 373 midline (raphe pallidus and raphe magnus) and a more lateral part centered on the lateral paragigantocellular
 374 nucleus (LPGi) and the Parapyramidal nucleus (PPy).

375

376 *Overall effect of muscimol microinjection within the RVM/rMR on the vasomotion of the tail*

377

378 During the control period, the tail was vasoconstricted, with a decreasing thermal gradient from $T_{\text{tail-prox}}$
 379 to $T_{\text{tail-dist}}$ [27.1 (26.9-27.3) vs. 24.9 (24.7-25.1)°C; $P < 0.001$]. The microinjection of muscimol within the
 380 RVM/rMR elicited an increase of the tail skin temperature. However, a proximal-distal gradient was also
 381 seen regarding the reactivity of the tail. Knowing these gradients, we analyzed the proximal and distal parts
 382 of the tail, separately, using the type of grouping already made but based on the starting point of the acute
 383 ascending phase of vasodilatation on the distal part of the tail (1st group (acute onset group): $0 < t_{\text{min}} < 7.5$
 384 min; 2nd group (intermediate onset group): $7.5 < t_{\text{min}} < 15$ min; 3rd group (late or none reactive): $t_{\text{min}} > 15$
 385 min), following sigmoidal adjustment of each individual. The corresponding temporal evolutions of adjusted
 386 skin temperatures are shown in Figure 6 for the 3 groups. Regarding the first two groups, the corresponding
 387 numerical data are provided in table 1B. By comparison with the paws the process was slower (in the 0.3-
 388 0.5°C/min range) and less pronounced (in the 4-6°C range), possibly because we recorded the dorsal facet of
 389 the tail (see discussion).

390 Figure 7 shows the corresponding localization of the muscimol microinjection sites for the proximal
 391 (Fig. 7A) and the distal (Fig. 7B) parts of the tail. Again, the black grey and white symbols represent the
 392 acute, intermediate and late or none reactive group respectively. The black symbols are located mainly
 393 between planes -1.3 and -2.8 mm, close to the midline, in the raphe pallidus and raphe magnus. The grey
 394 symbols surround the black ones and are located in the raphe magnus and parapyramidal region. In these two
 395 groups, the proximal and distal parts of the tail reacted concomitantly. Overall, the proximal part of the tail
 396 was more responsive to the microinjection; in particular, one can see several points from which a
 397 vasodilatation was elicited on the proximal but not on the distal part of the tail, at least within the 15-min
 398 early period. Most of these points were however located in the raphe magnus and parapyramidal nucleus.

399 Figure 8 represents the three-dimensional mapping of response latencies t_{min} as a function of
 400 injection site. For both the proximal (Fig. 8A) and the distal (Fig. 8B) parts of the tail, the earliest response
 401 latencies were observed between planes $z = -1.3$ and $z = -2.8$ mm from the midline (raphe pallidus and raphe
 402 magnus) and a more lateral part. Interestingly, the lateral part centered on the Parapyramidal nucleus was
 403 restricted to planes $z = -2.3$ to -2.8 mm without any obvious participation of the lateral paragigantocellular
 404 nucleus.

405

406 *Comparison of Heat Loss Indexes in various vasomotor states*

407

408 The potential extent of skin temperature variations was physically restricted to the $T_{\text{amb}}-T_{\text{core}}$ range.
 409 In terms of thermoregulation, these changes are best described using the Heat Loss Index as it eliminates the
 410 passive changes and range limitation due to any T_{amb} and T_{core} variations (Gordon et al. 2002; Romanovsky
 411 et al. 2002; Székely 1986): $\text{HLI} = (T_{\text{skin}}-T_{\text{amb}})/(T_{\text{core}}-T_{\text{amb}})$. Table 2 compares results of skin temperature,
 412 converted in terms of HLI, obtained in the present study (acute onset group 1, black symbols) to previous
 413 experiments performed on anesthetized rats maintained in thermo-neutral conditions (El Bitar et al. 2014a).
 414 The HLI values in the control period of the present study were close to those recorded during
 415 vasoconstrictions in our previous study and identical in terms of ranking ($T_{\text{tail-dist}} < T_{\text{paw-ipsi}} < T_{\text{tail-prox}}$).
 416 However, the HLI values following muscimol microinjection were 20-25% lower than the HLI seen during
 417 the maximal physiological vasodilatation achieved during thermo-neutrality. This observation suggests that
 418 the ongoing hind-paws and tail fiber sympathetic activity was not completely silenced following the
 419 muscimol microinjections, in spite of an apparent ceiling effect.

420

421 *Overall results, including the effects on vital signs*

422

423 In order to homogenize the results for further analyzes, the experiments were reorganized in three
 424 new groups, again on the basis of the onset time t_{min} of the ascending phase of vasodilatation (Fig. 9). The
 425 first includes experiments where t_{min} was < 15 min for all considered skin areas either on the tail or the paws
 426 (black circles in figure 9A). They were located between planes -0.8 and -2.8 mm, not more lateral than 0.3
 427 mm from the midline, mainly in the inner part of raphe magnus and raphe pallidus. The second includes
 428 experiments where t_{min} was < 15 min for at least one but not all the areas considered on the tail or the hind-
 429 paws (grey circles in figure 9A). They were located in the raphe magnus and parapyramidal area,
 430 surrounding the preceding group. The third group includes experiments where t_{min} was > 15 min for all
 431 considered skin areas either on the tail or the paws (white circles in figure 9A). The corresponding effects of
 432 microinjection of muscimol on $T_{\text{paw-ipsi}}$, $T_{\text{paw-contra}}$, $T_{\text{tail-prox}}$ and $T_{\text{tail-dist}}$ are summarized in figures 9B, C, D and
 433 E, respectively.

434 Figure 9F shows the concomitant effects on T_{core} . There was no statistical difference among the three
 435 groups concerning T_{core} during the control period ($P = 0.94$). After the muscimol injection, the mean
 436 temperatures diverged strongly with progressive drops for the 1st and 2nd group. The effects of muscimol
 437 microinjections on MAP, HR and ETCO_2 are presented in Figures 9G, H and I, respectively. For all three
 438 groups, we report a transitory increase of MAP and HR in the first minute following the microinjection of
 439 muscimol. Thereafter, the curves declined slowly and slightly till the end of the experiments. Regarding the
 440 first two groups, the corresponding numerical data are provided in table 3. These results are in line with
 441 previous reports in anesthetized rats following microinjection of muscimol in the RVM/rMR, describing
 442 slight or non-significant decreases in MAP, HR and ETCO_2 (Bernard et al. 2008; Blessing and Nalivaiko
 443 2001; Nakamura and Morrison 2007; Tanaka et al. 2007; Zaretsky et al. 2003a; 2003b). Note that our

444 recordings were made under an anesthetic regime that preserves withdrawal reflexes while most earlier
 445 reports were obtained with deeper regimes that could have masked the effects reported here.

446

447 ***Modeling the effect of muscimol injection within the RVM/rMR on the tail-flick test***

448

449 In a previous study, we proposed and verified experimentally a simple model to compute the
 450 expected tail-flick latency (TFL) of a rat exposed to a source of radiant heat applied onto the tail (Benoist et
 451 al. 2008). The model takes into account the power of the radiant heat source, the initial skin temperature, the
 452 core temperature and the site of stimulation on the tail, and has been applied successfully to reconstruct TFLs
 453 following a conditioned stress response (Carrive et al. 2011). Here, the model was used to compute the
 454 predictable variations of TFL introduced by muscimol. Decisional and motor latencies were estimated to be
 455 134 and 4 ms, respectively (Benoist et al. 2008). Considering a site of stimulation on the mid-tail, the
 456 distance to the dorsal horn entry zone is approximately 200 mm. The model provides the following equation
 457 for the expected tail-flick latency: $TFL (s) = [(36.8 - 0.73 \cdot T_{mid-tail})^2 / \alpha + 90 / (0.041 \cdot T_{core} - 0.47) +$
 458 $110 / (0.041 \cdot T_{mid-tail} - 0.47) + 138] / 1000$ where α is the slope of the squared temperature variation (in $^{\circ}C^2/s$)
 459 generated by the power of the radiant heat source.

460 Let us recall at this point that, when the skin is exposed to a constant power source of infrared
 461 radiation, the temperature increases with the square root of time, according to the law of radiant heat transfer
 462 $T = T_{mid-tail} + a \cdot t^{0.5}$ or, expressed in terms of temperature variation $T - T_{mid-tail} = a \cdot t^{0.5}$. This quadratic
 463 relationship becomes linear in t by squaring the two terms of the equation: $(T - T_{mid-tail})^2 = a^2 \cdot t = \alpha \cdot t$ where α
 464 is the slope of the squared temperature variation generated by the power of the radiant heat source [see Fig.
 465 2A in (Benoist et al. 2008)]. The predictive model of TFL was fully verified following variations of the
 466 radiant heat source (i.e. α) or the basal temperature of the skin (i.e. $T_{mid-tail}$ here) [see Fig. 8 in (Benoist et al.
 467 2008)]. In the classical tail-flick test, the principal source of variation introduced by experimenters is the
 468 power of the electrical bulb used for heating the skin of the animal. The investigator adjusts the radiant heat
 469 emission with a rheostat to achieve a predetermined TFL in the control situation, most commonly in the 2-4
 470 seconds range (Le Bars et al. 1999, 2009). In the model, such latencies are achieved for α in the 0.08-
 471 $0.2^{\circ}C^2/s$.

472 The model was applied to the data of animals in which the beginning of the ascending phase of
 473 vasodilatation was < 15 min either on the tail or the paws (black group in figure 9). The model foretells a 30-
 474 35% decrease of the TFL, thirty minutes following muscimol administration (Fig. 10). It appears therefore
 475 that, regardless of any other additional possible causes, the vasodilatation of the tail is a major source of
 476 variation of the TFL following muscimol administration in RVM/rMR.

477

478 **DISCUSSION**

479

480 Muscimol was injected in the lower brainstem with the aim of assessing the role of the RVM/rMR
481 on the control of sympathetic drive to the tail and hind-paws. Microinjections within this brainstem region
482 increased the skin temperature of the hind-paws and tail as a result of reduced vasomotor tone. The effects
483 were dominant on the hind-paw ipsilateral to the microinjection site. Increased heat loss through
484 vasodilatation of the tail and paws were associated with a drop of T_{core} and slight decreases of MAP, HR and
485 ETCO_2 .

486 Following some technical considerations regarding the microinjection procedure, we will discuss the
487 following points: (1) general findings; (2) lateral localization of effective sites; (3) rostro-caudal localization
488 of effective sites; (4) pharmacological manipulations of RVM/rMR in pain studies.

489

490 ***Technical considerations regarding the microinjection procedure***

491

492 The kinetic and volume of efficient microinjection is determined by numerous factors: the
493 concentration, rate of delivery and properties of both the drug - coefficient of diffusion, binding, catabolism -
494 and the tissue - volume fraction, tortuosity - (Syková and Nicholson 2008). In nuclear and cortical
495 homogenous regions, drug distributions are typically spherical or in the shape of drop (Bondareff et al. 1970;
496 Martin 1991; Myers 1966).

497 In a “mapping” study aiming at demarcating a functional region in the brain, both positive and
498 negative results are significant. A negative result obtained with a large dose is a very convincing result in
499 this respect. Considering the large volume of the explored brain structure (roughly $3 \times 4 \times 2 = 24 \text{ mm}^3$), a
500 compromise was necessary to both find significant positive results with minimal doses and to avoid useless
501 negative results. Studies on the involvement of these regions in pain/nociception and thermoregulation have
502 used muscimol injections in the 10-1000 pmol / 60-1000 nl ranges (Bernard et al. 2008; Blessing and
503 Nalivaiko 2001; Brink et al. 2006; Cao et al. 2004, 2010; Cerri et al. 2010; Fan et al. 2007. Gilbert and
504 Franklin 2001; Heinricher and Kaplan, 1991; Martenson et al. 2009. Meng et al. 1998; Morrison 1999, 2003;
505 Nakamura and Morrison 2007, 2011; Ootsuka and McAllen 2005; Rathner et al. 2008; Vianna et al. 2008;
506 Zaretsky et al. 2003a, 2003b). Knowing that muscimol does not spread appreciably because it is a potent
507 ligand for neuronal and glial GABA_A receptors, we decided to use a small volume of injection ($50 \text{ nl} = 0.05$
508 mm^3 , that is a $\sim 0.5 \text{ mm}$ diameter for an ideal sphere) but a relatively high concentration. This was supposed
509 to provide an effective radius of blockade in the $\sim 1 \text{ mm}$ range (Martin 1991; Martin and Ghez 1999; Malpeli
510 1999; Edeline et al. 2002). Following similar microinjections using [^3H]muscimol, autoradiographic analyses
511 showed a spread $\sim 1.5 \text{ mm}$ from the injection site at 15 min (Edeline et al. 2002; Martin 1991). Martin and
512 Ghez (1999) used glucose metabolism to assess the extent of inactivation and observed a central core of
513 blockade ($\sim 1 \text{ mm}$ radius) surrounded by an extensive region of reduced metabolism, possibly due to reduced
514 synaptic activity of neurons receiving projections from the core region. In summary, muscimol binds

515 strongly and diffuses slowly outward at effective concentrations from the region immediately inundated by
516 the bulk flow (Malpeli 1999).

517 Since myelinated fiber bundles impede muscimol diffusion (Allen et al. 2008), it is likely that the
518 particular architecture of the RVM/rMR with a predominance of rostral-caudal fibers and a low neuronal
519 density favors a rostral-caudal diffusion of the product. In addition, the two paired bundles of myelinated
520 fibers that cover the brainstem floor, namely the pyramidal tract and the medial lemniscus, constitute a
521 strong diffusion barrier. Accordingly, the post-mortem examination of pontamine spread revealed an
522 elongated pattern of diffusion two times longer in the rostral-caudal direction as compared to the coronal
523 plane.

524 Using these microinjections, we were able to build response maps on the basis of 160 experiments.
525 Together with the small volume of injection and the large number of negative sites of injection (60%), this
526 approach provided (1) an acute delineation of the structures able to block sympathetic cutaneous
527 vasoconstrictor activity; (2) the possibility of a temporal analysis of these effects; and (3) the resultant
528 capacity of defining a brain region as the core of effects, surrounded by intermediate and then ineffective
529 zones.

530 Because of such a large number of injection sites, we introduced a new procedure to compute three-
531 dimensional interpolated maps of response latencies and overall sympathetic blockade as a function of
532 injection site. The interpolation was performed by computing an average of the responses obtained at all
533 injection sites, weighted by the distance between the interpolated voxel and each injection site. This ensured
534 that the interpolated values were most dependent on the responses of the nearest injection sites. In addition,
535 because of the non-homogeneous sampling of the interpolated volume, a mask was used to exclude voxels
536 that were not close to at least one injection point. The obtained volumes provide an interesting mean to
537 assess the relationship between the effects of the injection and the anatomical location of the injection.

538

539 ***General findings***

540

541 Our results are largely in agreement with earlier reports regarding the sympathetic drive of the tail.
542 Microinjection of glycine, GABA or muscimol in the RVM/rMR blocks the activation by cold or fever of
543 sympathetic fibers that innervate the tail (Blessing and Nalivaiko 2001; Cerri et al. 2010; Korsak and Gilbey
544 2004; Ootsuka and McAllen 2005; Ootsuka et al. 2004; Rathner et al. 2008; Vianna et al. 2008). On the other
545 hand, microinjection of glutamate or bicuculline increases the activity of vasomotor sympathetic nerves of
546 the tail, thus decreasing the blood flow, without affecting the mesenteric vascular bed (Blessing and
547 Nalivaiko 2001; Morrison 2001; Rathner and McAllen 1999). Several aspects of our contribution should be
548 highlighted.

549 The experimental conditions were close to those of thermoneutrality (El Bitar et al. 2014a). T_{warm} was
550 adjusted to $\sim 0.3^{\circ}\text{C}$ below T_{core} . Demonstrating their vasoconstricted state, the temperature of the distal part
551 of the tail was very close to the ambient temperature ($\sim 0.7^{\circ}\text{C}$ above T_{ambient}). It then increased by $\sim 6^{\circ}\text{C}$
552 following the injection of muscimol in responsive brainstem sites. In comparable experimental conditions,

553 microinjection of GABA or muscimol in RVM/rMR blocks the activity of the sympathetic fibers innervating
554 the rat tail (Korsak and Gilbey 2004; Ootsuka and McAllen 2005).

555 We have previously discussed (El Bitar et al. 2014a) that the vasomotor tone of the dorsal facet of
556 the tail is less reactive than the ventral facet, notably because the ventral artery is larger than the lateral
557 arteries, while the ventral vein is thinner than the lateral veins (Knoppers 1942; Thorington 1966; Wu et al.
558 1995; Young and Dawson 1982). It follows that the temperatures of the dorsal and ventral facets of the tail
559 are identical during vasoconstriction but shift by $\sim 3^{\circ}\text{C}$ during full vasodilatation. The recorded effects from
560 the tail were thus underestimated, as compared to those seen on the hind paws.

561 A major novelty of our study was to include the paws to these basic phenomenological observations.
562 Such as for the tail, the hind-paws were in a stable vasoconstricted state, as demonstrated by the fact that the
563 temperature of the hind-paws was close to the ambient temperature ($2\text{-}3^{\circ}\text{C}$ above T_{ambient}). This increased by
564 $\sim 7^{\circ}\text{C}$ following the injection of muscimol in the active sites. We have already discussed the involvement of
565 the paws in rat thermoregulation (El Bitar et al. 2014a). The feet make up approximately 10% of the total
566 surface area of the body, slightly more than the tail (Lin et al. 1979). It follows that the substantial muscimol-
567 induced vasodilatation of the paws contributed significantly to the core temperature drop ($\sim 1^{\circ}\text{C}$ within half
568 an hour).

569 Our purpose was not to confirm well-documented notions. We specifically aimed at mapping the
570 brainstem regions that contain the premotor sympathetic neurons that control the vasomotor tone of the tail
571 and hind-paws because most models of pain/nociception are based on behavioral responses elicited by
572 *thermal* stimulation (reviewed in Le Bars et al. 2001, 2009). We undertook this large study because studies
573 on pain/nociception have emphasized the Rostral Ventromedial Medulla (RVM), which includes the nucleus
574 raphe magnus and the gigantocellular reticular nucleus pars alpha (mainly at the level of the facial nucleus),
575 while studies on thermoregulation have emphasized a slightly shifted more caudal region centered on the
576 raphe pallidus. In addition, we described in a previous work that neurons involved in pain/nociception
577 located in the brainstem are probably also implicated in autonomic regulation, notably cutaneous vasomotion
578 (El Bitar et al. 2014b).

579 The results of the present study suggest that the regions described as being involved in
580 pain/nociception modulation and the regions involved in thermoregulation are spatially matched, at least
581 functionally regarding the vasomotor tone of the tail and hind-paws.

582

583 *Localization of effective sites in coronal planes*

584

585 The most effective sites were restricted to well-circumscribed regions. Numerous negative
586 microinjections sharpened the delineation. Our observations regarding the tail are in keeping with the
587 mapping by Korsak and Gilbey (2004) who reported that GABA microinjections in the region of raphe
588 pallidus and magnus markedly decreased the sympathetic cutaneous vasoconstrictor activity in the dorsal
589 collector nerves of the tail, while injections more dorsal or lateral tended to produce either a smaller decrease

590 or have no effect. Blessing and Nalivaiko (2001) also emphasized the raphe magnus, raphe pallidus and
591 parapyramidal nucleus in this respect, although they did not provide a graphical mapping of the effects.

592 Only microinjections in RMg, RPa and PPy elicited a vasodilatation in the ipsilateral hind-paw
593 within less than 7.5 min and those distant from the midline by less than 0.3 mm induced a vasodilatation in
594 the contralateral hind-paw within the same period. These observations deserve two comments. First, within
595 the coronal plane, the lateral diffusion of muscimol was limited, as expected. Second, projections of
596 RVM/rMR cells are mainly lateralized, predominantly controlling vasomotor tone of the ipsilateral body
597 side. Our results are in keeping with studies showing that RVM/rMR neurons send axons towards the spinal
598 cord mainly through the ipsilateral dorso-lateral funiculus (Basbaum and Fields 1979; Fields et al. 1995;
599 Lefler et al. 2008; Light 1985). Microinjections close to the midline also elicited early vasodilatation of the
600 tail, the most effective sites being restricted to the same well-circumscribed regions. Neurons in the PPy
601 present morphological, histo-chemical (Helke et al. 1989; Lynn et al. 1991) and functional (Blessing and
602 Nalivaiko 2000) properties similar to those of the RPa. Some authors consider therefore PPy as part of RPa
603 (e.g. Cano et al. 2003).

604 Interestingly, brainstem neurons activated both antidromically from the lumbar dorso-lateral
605 funiculus and by mild cooling of the animal core temperature, were found in both raphe pallidus and magnus
606 (Rathner et al. 2001). Such neurons could be involved in the results presented here. However, there are other
607 control loops that regulate the central temperature through the vessels in the hairy skin, the interscapular
608 brown adipose tissue (BAT) and the fusimotor fibers to limb muscles, all being silenced by neuronal
609 inhibition of the raphe pallidus and/or magnus (McAllen et al. 2010). Although they all should have a
610 sympathetic premotor relay in these nuclei, these four sympathetic thermo-effector outflows differ in terms
611 of thermal thresholds, relative responsiveness to core temperature, patterns and driving by neural pathways,
612 and thus probably do not “crosstalk” at this level (McAllen et al. 2010; Nagashima et al. 2000; Ootsuka and
613 McAllen, 2006 ; Romanovsky 2007 ; Tanaka et al. 2007). The relative contribution of single individual
614 neurons to these functions remains an open question.

615

616 ***Rostro-caudal localization of effective sites***

617

618 Overall, the injection sites which elicited the most widespread and early latency vasodilation were
619 located in the coronal planes posterior to the interaural line by 1.3-2.6 mm. 85% of experiments where the
620 vasodilatation of all areas either on the tail or the paws occurred in less than 15 min were found in these
621 regions. Again our observations agree with the report by Korsak and Gilbey (2004) showing a similar rostro-
622 caudal extension of their effective sites for blocking by GABA the sympathetic vasoconstrictor drive in the
623 tail. Similarly, brainstem neurons both antidromically activated from the lumbar dorso-lateral funiculus and
624 activated by mild cold were found in the raphe nuclei between the coronal planes posterior to the interaural
625 line by 1.8-2.3 mm (Rathner et al. 2001).

626 Overall, the literature related to thermoregulation points to coronal planes immediately rostral to the
627 rostral pole of the inferior olivary complex at the level of the caudal half of the facial nucleus. This brainstem

628 region is often referred as to the rostral raphe pallidus, although it generally does include the nucleus raphe
 629 magnus (e.g. Madden and Morrison 2003, 2005; Morrison 1999, 2003; Morrison et al. 1999, 2000; Rathner
 630 et al. 2008). In fact, very few studies were devoted to a systematic mapping.

631 As pointed out by Nason and Mason (2004), it is unlikely that a microinjection into any single
 632 nucleus in RVM/rMR will affect neurons confined to that nucleus because these neurons have large dendritic
 633 arbors that cross cytoarchitectonic boundaries (Gao and Mason 1997; Mason et al. 1990; Newman 1985;
 634 Potrebic and Mason 1993). Blessing (2003) discussed the conventional anatomical demarcation into RMg
 635 and RPa by raising the following points. The delimitation of boundaries is based particularly on the work of
 636 Taber et al. (1960) that follows the atlas of Meessen and Olszewski (1949) for rabbits and the atlas of
 637 Olszewski and Baxter (1954) for humans. However, the rabbit atlas combines all the ventral midline neurons
 638 in the rostral medulla and caudal pons as “RMg” and does not use the term “RPa.” In contrast, the human
 639 atlas uses “RPa” and not “RMg”. However, by convention, RMg in the rat is more rostral and dorsal, and
 640 RPa is more caudal and ventral (Paxinos and Watson 2005).

641 We noted that the Heat loss Indexes following muscimol microinjection were 20-25% lower than the
 642 HLI seen during the maximal physiological vasodilatation achieved in rats maintained in thermo-neutral
 643 conditions (El Bitar et al. 2014a), suggesting that the ongoing hind-paws and tail fiber sympathetic activities
 644 were not completely silenced following the microinjections, in spite of a clear ceiling effect when
 645 microinjections were effective. The most parsimonious explanation for this observation is the oblong
 646 geometry of the involved brainstem structures, ~12 times longer than the diameter of the injected volume,
 647 preventing the drug to reach all structures potentially involved in controlling vasomotor tone.

648 In summary, there are morphological and functional reasons to consider the RVM and rMR nuclei as
 649 a single RVM/rMR entity, as already proposed by Mason et al. (2001, 2005a, 2005b, 2006, 2011).

650

651 *Is the RVM really specific for pain/nociception?*

652

653 Our study shows, in the rat, a mutual covering of the regions involved in thermoregulation (at least,
 654 regarding the vasomotor tone of the tail and hind-paws) with those reported as being specifically involved in
 655 pain/nociception.

656 In spite of several warnings initiated by Thelma Lovick and Peggy Mason (Le Bars et al. 2001;
 657 Lefler et al. 2008; Lovick 1997; Mason 2001; 2005a; 2005b; 2006; 2011; 2012), the specificity of the RVM
 658 regarding the control of pain/nociception mechanisms is repeatedly put forward or assumed (e.g. Fields et al.
 659 2006; Heinricher and Ingram, 2008; Basbaum et al. 2009; Heinricher et al. 2009). RVM neurons do not only
 660 project towards the dorsal horn of the spinal cord (Fields and Basbaum 1978; 1999), but also to the
 661 intermediolateral cell column, with a high degree of collateralization in both the rostro-caudal and dorso-
 662 ventral axes (Bacon et al. 1990; Basbaum et al. 1978; Hossaini et al. 2012; Lefler et al. 2008; Loewy 1981;
 663 Morrison and Gebber 1985).

664 Numerous neurons in RVM/rMR were identified as sympathetic premotor neurons by early
 665 retrograde trans-synaptic labeling with the pseudo-rabies virus (Smith et al. 1998; Strack et al. 1989).

666 Quantitative data, obtained from 6 days survival experiments, revealed ~5 times more labeled neurons in
667 raphe magnus and gigantocellular reticular pars alpha nuclei than within the raphe palidus nucleus (Smith et
668 al. 1998). Smith et al. (1998) found the highest density at the level of the facial nucleus but the coronal
669 planes facing the rostral part of the facial nucleus were not represented. Therefore, the neurons labeled in
670 that study could have been mainly located in the RVM/rMR at the level of facial nucleus, although we
671 cannot infer their rostral extent. However, it was stated more recently that transneuronally labeled neurons
672 are distributed through the parapyramidal region, including all RVM/rMR elements (Tóth et al. 2006), at
673 least within the coronal planes from 1.3 to 3.3 mm posterior to the interaural line (Nakamura et al., 2004).
674 Finally, cold exposure increases the expression of Fos immunoreactivity not only in RPa and PPy (Bonaz
675 and Taché 1994; Cano et al. 2003; Martinez et al. 2001; Morrison et al. 1999) but also in RMg, between the
676 coronal planes posterior to the interaural line by 1.3-3.3 mm (Nakamura et al., 2004).

677 If one moves back to the literature related to nociception, namely the so-called “on-“ and “off-“ cells
678 recorded within the medial brainstem, one is struck by the similar rostro-caudal distribution of the sites, all
679 pointing out the coronal planes including the facial nucleus. Interestingly, Vanegas et al. (1984) attempted to
680 map “on-“ and “off-“ neurons that project to the spinal cord, and found that these were located in brain
681 regions 1.9-2.7 mm posterior to the interaural line. In summary, the most effective sites for blocking by
682 muscimol the cutaneous vasoconstrictor fibers matches exactly the brainstem sites where “on-“ and “off-“
683 cells were recorded over the last years, notably those projecting to the spinal cord.

684

685 *Pharmacological manipulations of RVM/rMR in pain studies*

686

687 Administration of muscimol exclusively within RVM/rMR results in a significant decrease in TFL
688 while administration of the competitive GABA_A receptor antagonist bicuculline (but not the glycine receptor
689 antagonist strychnine) induces an increase of the TFL (Drower and Hammond 1988; Gilbert and Franklin
690 2001; Heinricher and Kaplan 1991; Heinricher and Tortorici 1994; Nason and Mason 2004). Similar results
691 have been reported with paw withdrawal and hot-plate tests (Gilbert and Franklin 2001; Martenson et al.
692 2009).

693 These increases or decreases of TFL are generally interpreted in terms of hypo- or hyper-algesia,
694 respectively. However, other interpretations are conceivable, available and advisable. The tail-flick test does
695 not achieve the criterion of construct validity because it does not effectively measure the targeted construct,
696 i.e. a quantitative nociceptive response, presumed to reflect an animal's perception of pain (Le Bars et al.
697 2001, 2009). Indeed, the reaction time measured in the conventional tail-flick test (and all other tests using
698 conventional progressive heating) is the sum of (1) the time to achieve the threshold for the behavioral
699 reaction and (2) the behavioral latency (Benoist et al. 2008; Pinedé et al. 2012). If the reaction time is the
700 only measured end-point, there is no way of knowing whether the variation was produced by changes of
701 either the basal skin temperature or the threshold temperature, or both. Using a simple model for computing
702 the TFL in the rat, taking into account the power of the radiant heat source, the initial skin temperature, the
703 core temperature and the site of stimulation on the tail (Benoist et al. 2008), we predicted that the change in

704 tail temperature 15 minutes after effective muscimol injection would lead to a 30-35% reduction of the TFL.
705 Interestingly, Heinricher and Kaplan (1991) described a decrease of the TFL of approximately 30% at 12
706 min post-injection of muscimol (50 ng; 0.5 μ l), maintained throughout the half an hour observation period, a
707 finding reproduced by Meng et al. (1998). Both observations match remarkably the predicted variations of
708 TFL related to changes in baseline skin temperature. Interestingly, Tjølsen and Hole (1997) attributed the
709 reduction of TFL following lesions of the raphe-spinal serotonergic system to the increase in skin
710 temperature.

711 It should be noted that such considerations are not restricted to the tests based on the utilization of
712 thermal stimuli. For example, the vasodilatation of the paws induced by high ambient temperatures
713 exacerbates the second phase of the formalin test (Rosland 1991; Tjølsen et al. 1992). It follows that the
714 increased responsiveness to formalin injection following muscimol administration in RVM/rMR (Gilbert and
715 Franklin 2001) could also be largely due to the unavoidable vasodilatation.

716

717 ***Conclusion***

718

719 The functional blockade of the RVM/rMR by muscimol elicits an important increase of skin
720 temperature of the paws and tail, eliciting a reduction of the core temperature. The effective zones match
721 very exactly the brain regions defined as specifically devoted to the control of nociception. Because changes
722 in skin temperature can have a strong effect on the usual tests of pain using radiant heat such as the TFL, our
723 results indicate that the evidence that pharmacological manipulations of RVM/rMT modulate pain-specific
724 descending modulatory pathways could, actually, be explained by unaccounted changes in vasomotor tone.

725

726

727 **ACKNOWLEDGMENTS**

728 We thank Professors Pascal Carrive, François Cesselin and Léon Plaghki for advice in the preparation of the
729 manuscript. Nabil El Bitar was supported by a grant from the Société Française d'Etude et de Traitement de
730 la Douleur (SFETD) et l'Institut UPSA de la douleur (IUD).

731

732 **AUTHOR CONTRIBUTIONS**

733 Conceived and designed the experiments: NEB, BP, DLB. Performed the experiments: NEB, BP, DLB.
734 Analyzed the data: NEB, BP, DLB, AM, GH. Wrote the paper: NEB, BP, AM, DLB.

735

736

737 REFERENCES

738

739 **Allen TA, Narayanan NS, Kholodar-Smith DB, Zhao Y, Laubach M, Brown TH.** Imaging the spread of
740 reversible brain inactivations using fluorescent muscimol. *J Neurosci Methods* 171: 30-38, 2008.

741 **Bacon SJ, Zagon A, Smith AD.** Electron microscopic evidence of a monosynaptic pathway between cells in
742 the caudal raphe nuclei and sympathetic preganglionic neurons in the rat spinal cord. *Exp Brain Res* 79:
743 589-602, 1990.

744 **Barbaro NM, Heinricher MM and Fields HL.** Putative nociceptive modulatory neurons in the rostral
745 ventromedial medulla of the rat display highly correlated firing patterns. *Somatosens Mot Res* 6: 413-425,
746 1989.

747 **Basbaum AI, Fields HL.** The origin of descending pathways in the dorsolateral funiculus of the spinal cord
748 of the cat and rat: further studies on the anatomy of pain modulation. *J Comp Neurol* 187: 513-531, 1979.

749 **Basbaum AI, Clanton CH, Fields HL.** Three bulbospinal pathways from the rostral medulla of the cat: an
750 autoradiographic study of pain modulating systems. *J Comp Neurol* 178: 209-224, 1978.

751 **Basbaum AI, Braz J, Ossipov MH, Porreca F.** The endogenous neuromodulation system. In:
752 Neuromodulation, edited by Krames E, Peckham PH and Rezai A. London, Burlington, San Diego:
753 Academic Press, 2009, p. 303-312.

754 **Beaumont K, Chilton WS, Yamamura HI, Enna SJ.** Muscimol binding in rat brain: association with
755 synaptic GABA receptors. *Brain Res* 148: 153-162, 1978.

756 **Benoist J-M, Pinedé I, Ballantyne K, Plaghki L, Le Bars D.** Peripheral and central determinants of a
757 nociceptive reaction: an approach to psychophysics in the rat. *PLoS ONE* 3: e3125, 2008.

758 **Bernard J-F, Netzer F, Gau R, Hamon M, Laguzzi R, Sévoz-Couche C.** Critical role of B3 serotonergic
759 cells in baroreflex inhibition during the defense reaction triggered by dorsal periaqueductal gray
760 stimulation. *J Comp Neurol* 506:108-121, 2008.

761 **Blessing WW.** Lower brainstem pathways regulating sympathetically mediated changes in cutaneous blood
762 flow. *Cell Mol Neurobiol* 23: 527-538, 2003.

763 **Blessing WW, Nalivaiko E.** Cutaneous vascular bed is not involved in arterial pressure changes elicited by
764 increasing or decreasing the activity of inhibitory vasomotor neurons in caudal ventrolateral medulla in
765 rabbits. *Neurosci Lett* 290: 141-144, 2000.

766 **Blessing WW, Nalivaiko E.** Raphe magnus/pallidus neurons regulate tail but not mesenteric arterial blood
767 flow in rats. *Neuroscience* 105: 923-929, 2001.

768 **Blessing WW, Yu YH, Nalivaiko E.** Raphe pallidus and parapyramidal neurons regulate ear pinna vascular
769 conductance in the rabbit. *Neurosci Lett* 270: 33-36, 1999.

770 **Bonaz B, Taché Y.** Induction of Fos immunoreactivity in the rat brain after cold-restraint induced gastric
771 lesions and fecal excretion. *Brain Res* 652: 56-64, 1994.

772 **Bondareff W, Routtenberg A, Narotzky R, McLone DG.** Intrastratial spreading of biogenic amines. *Exp*
773 *Neurol* 28: 213-229, 1970.

774 **Brink TS, Hellman KM, Lambert AM, Mason P.** Raphe magnus neurons help protect reactions to visceral
775 pain from interruption by cutaneous pain. *J Neurophysiol* 96: 3423-3432, 2006.

776 **Cano G, Passerin AM, Schiltz JC, Card JP, Morrison SF, Sved AF.** Anatomical substrates for the central
777 control of sympathetic outflow to interscapular adipose tissue during cold exposure. *J Comp Neurol* 460:
778 303-326, 2003.

779 **Cao WH, Morrison SF.** Disinhibition of rostral raphe pallidus neurons increases cardiac sympathetic nerve
780 activity and heart rate. *Brain Res* 980: 1-10, 2003.

781 **Cao WH, Fan W, Morrison SF.** Medullary pathways mediating specific sympathetic responses to
782 activation of dorsomedial hypothalamus. *Neuroscience* 126: 229-240, 2004.

- 783 **Cao WH, Madden CJ, Morrison SF.** Inhibition of brown adipose tissue thermogenesis by neurons in the
784 ventrolateral medulla and in the nucleus tractus solitarius. *Am J Physiol Regul Integr Comp Physiol* 299:
785 R277-R290, 2010.
- 786 **Carlson JD, Maire JJ, Martenson ME, Heinricher MM.** Sensitization of pain-modulating neurons in the
787 rostral ventromedial medulla after peripheral nerve injury. *J Neurosci* 27: 13222-13231, 2007.
- 788 **Carrive P, Churyukanov M, Le Bars D.** A reassessment of stress-induced "analgesia" in the rat using an
789 unbiased method. *Pain* 152: 676-686, 2011.
- 790 **Cerri M, Zamboni G, Tupone D, Dentico D, Luppi M, Martelli D, Perez E, Amici R.** Cutaneous
791 vasodilation elicited by disinhibition of the caudal portion of the rostral ventromedial medulla of the free-
792 behaving rat. *Neuroscience* 165: 984-995, 2010.
- 793 **Covino BG, Dubner R, Gybels J, Kosterlitz HW, Liebeskind JC, Sternbach RA, Vycklický L,
794 Yamamura H, Zimmermann M.** Ethical standards for investigations of experimental pain in animals.
795 The Committee for Research and Ethical Issues of the International Association for the Study of Pain.
796 *Pain* 9: 141-143, 1980.
- 797 **Drower EJ, Hammond DL.** GABAergic modulation of nociceptive threshold: effects of THIP and
798 bicuculline microinjected in the ventral medulla of the rat. *Brain Res* 450: 316-324, 1988.
- 799 **Edeline JM, Hars B, Hennevin E, Cotillon N.** Muscimol diffusion after intracerebral microinjections: a
800 reevaluation based on electrophysiological and autoradiographic quantifications. *Neurobiol Learn Mem*
801 78: 100-124, 2002.
- 802 **El Bitar N, Pollin B, Karroum EG, Pinedé I, Mouraux A, Le Bars D.** Thermoregulatory vasomotor tone
803 of the rat tail and paws in thermoneutral conditions and its impact on a behavioral model of acute pain. *J*
804 *Neurophysiol* 112: 2185-2198, 2014a.
- 805 **El Bitar N, Pollin B, Le Bars D.** "On-" and "off-" cells in the Rostral Vento-medial Medulla of rats held in
806 thermo-neutral conditions: are they involved in thermoregulation? *J Neurophysiol* 112: 2199-2217,
807 2014b.
- 808 **Enna SJ, Snyder SH.** Properties of gamma-aminobutyric acid (GABA) receptor binding in rat brain
809 synaptic membrane fractions. *Brain Res* 100: 81-97, 1975.
- 810 **Fan W, Morrison SF, Cao WH, Yu P.** Thermogenesis activated by central melanocortin signaling is
811 dependent on neurons in the rostral raphe pallidus (rRPa) area. *Brain Res* 1179: 61-69, 2007.
- 812 **Fields HL, Basbaum AI.** Brainstem control of spinal pain-transmission neurons. *Annu Rev Physiol* 40: 217-
813 248, 1978.
- 814 **Fields HL, Basbaum AI.** Central nervous system mechanisms of pain modulation. In: Textbook of Pain,
815 edited by Wall PD and Melzack R. London: Churchill Livingstone, 1999, p. 309-329.
- 816 **Fields HL, Bry J, Hentall I and Zorman G.** The activity of neurons in the rostral medulla of the rat during
817 withdrawal from noxious heat. *J Neurosci* 3: 2545-2552, 1983.
- 818 **Fields HL, Malick A, Burstein R.** Dorsal horn projection targets of ON and OFF cells in the rostral
819 ventromedial medulla. *J Neurophysiol* 74: 1742-1759, 1995.
- 820 **Fields HL, Basbaum AI, Heinricher MM.** Central nervous system mechanisms of pain modulation. In:
821 Wall and Melzack's Textbook of Pain, edited by McMahon SB and Koltzenburg M. Edinburgh: Elsevier
822 Churchill Livingstone, 2006, p. 125-142.
- 823 **Gallagher JP, Nakamura J, Shinnick-Gallagher P.** Effects of glial uptake and desensitization on the
824 activity of gamma-aminobutyric acid (GABA) and its analogs at the cat dorsal root ganglion. *J*
825 *Pharmacol Exp Ther* 226: 876-884, 1983.
- 826 **Gao K, Mason P.** Somatodendritic and axonal anatomy of intracellularly labeled serotonergic neurons in the
827 rat medulla. *J Comp Neurol* 389: 309-328, 1997.
- 828 **Gilbert AK, Franklin KB.** GABAergic modulation of descending inhibitory systems from the rostral
829 ventromedial medulla (RVM). Dose-response analysis of nociception and neurological deficits. *Pain* 90:
830 25-36, 2001.

- 831 **Gordon CJ, Puckett E, Padnos B.** Rat tail skin temperature monitored noninvasively by radiotelemetry:
832 characterization by examination of vasomotor responses to thermomodulatory agents. *J Pharmacol*
833 *Toxicol Methods* 47: 107-114, 2002.
- 834 **Heinricher MM, Ingram SL.** The brainstem and nociceptive modulation. In: The senses: a comprehensive
835 reference, edited by Basbaum AI, Akimichi K, Gordon MS and Westheimer G. Elsevier Academic Press,
836 2008, p. 593–626.
- 837 **Heinricher MM, Kaplan HJ.** GABA-mediated inhibition in rostral ventromedial medulla: role in
838 nociceptive modulation in the lightly anesthetized rat. *Pain* 47: 105-113, 1991.
- 839 **Heinricher MM, Tortorici V.** Interference with GABA transmission in the rostral ventromedial medulla:
840 disinhibition of off-cells as a central mechanism in nociceptive modulation. *Neuroscience* 63: 533-546,
841 1994.
- 842 **Heinricher MM, Tavares I, Leith JL, Lumb BM.** Descending control of nociception: Specificity,
843 recruitment and plasticity. *Brain research reviews* 60: 214–225, 2009.
- 844 **Helke CJ, Thor KB, Sasek CA.** Chemical neuroanatomy of the parapyramidal region of the ventral medulla
845 in the rat. *Prog Brain Res* 81: 17-28, 1989.
- 846 **Hertzman AB.** Some relations between skin temperature and blood flow. *Am J Phys Med* 32: 233-251,
847 1953.
- 848 **Hikosaka O, Wurtz RH.** Modification of saccadic eye movements by GABA-related substances. I. Effect
849 of muscimol and bicuculline in monkey superior colliculus. *J Neurophysiol* 53: 266-291, 1985.
- 850 **Hossaini M, Goos JA, Kohli SK, Holstege JC.** Distribution of glycine/GABA neurons in the ventromedial
851 medulla with descending spinal projections and evidence for an ascending glycine/GABA projection.
852 *PLoS ONE* 7: e35293, 2012.
- 853 **Kaplan H, Fields HL.** Hyperalgesia during acute opioid abstinence: evidence for a nociceptive facilitating
854 function of the rostral ventromedial medulla. *J Neurosci* 11: 1433-1439, 1991.
- 855 **Knoppers AT.** La queue du rat, témoin de la régulation thermique. *Arch Néer Physiol* 26: 364-406, 1942.
- 856 **Korsak A, Gilbey MP.** Rostral ventromedial medulla and the control of cutaneous vasoconstrictor activity
857 following i.c.v. prostaglandin E₁. *Neuroscience* 124: 709-717, 2004.
- 858 **Krogsgaard-Larsen P, Johnston GA, Lodge D, Curtis DR.** A new class of GABA agonist. *Nature* 268:
859 53-55, 1977.
- 860 **Le Bars D, Gozariu M, Cadden SW.** Animal models of nociception. *Pharmacol Rev* 53: 597-652, 2001.
- 861 **Le Bars D, Hansson P, Plaghki L.** Current animal test and models of pain. In: Pharmacology of Pain,
862 edited by Beaulieu P, Lussier D, Porreca F and Dickenson AH. Seattle: IASP Press, 2009, p. 475-504.
- 863 **Lefler Y, Arzi A, Reiner K, Sukhotinsky I, Devor M.** Bulbosplinal neurons of the rat rostromedial medulla
864 are highly collateralized. *J Comp Neurol* 506: 960-978, 2008.
- 865 **Light AR.** The spinal terminations of single, physiologically characterized axons originating in the
866 pontomedullary raphe of the cat. *J Comp Neurol* 234: 536-548, 1985.
- 867 **Lin MT, Chern YF, Liu GG, Chang TC.** Studies on thermoregulation in the rat. *Proc Natl Sci Counc R O*
868 *C* 3: 46-52, 1979.
- 869 **Loewy AD.** Raphe pallidus and raphe obscurus projections to the intermediolateral cell column in the rat.
870 *Brain Res* 222: 129-133, 1981.
- 871 **Lovick TA.** The medullary raphe nuclei: a system for integration and gain control in autonomic and
872 somatomotor responsiveness? *Exp Physiol* 82: 31-41, 1997.
- 873 **Lynn RB, Kreider MS, Miselis RR.** Thyrotropin-releasing hormone-immunoreactive projections to the
874 dorsal motor nucleus and the nucleus of the solitary tract of the rat. *J Comp Neurol* 311: 271-288, 1991.
- 875 **Madden CJ, Morrison SF.** Excitatory amino acid receptor activation in the raphe pallidus area mediates
876 prostaglandin-evoked thermogenesis. *Neuroscience* 122: 5-15, 2003.

- 877 **Madden CJ, Morrison SF.** Hypoxic activation of arterial chemoreceptors inhibits sympathetic outflow to
878 brown adipose tissue in rats. *J Physiol (Lond)* 566: 559-573, 2005.
- 879 **Malpeli JG.** Reversible inactivation of subcortical sites by drug injection. *J Neurosci Methods* 86: 119-128,
880 1999.
- 881 **Martenson ME, Cetas JS, Heinricher MM.** A possible neural basis for stress-induced hyperalgesia. *Pain*
882 142: 236-244, 2009.
- 883 **Martin JH.** Autoradiographic estimation of the extent of reversible inactivation produced by microinjection
884 of lidocaine and muscimol in the rat. *Neurosci Lett* 127: 160-164, 1991.
- 885 **Martin JH, Ghez C.** Pharmacological inactivation in the analysis of the central control of movement. *J*
886 *Neurosci Methods* 86: 145-159, 1999.
- 887 **Martínez V, Wang L, Taché Y.** Central TRH receptor 1 antisense blocks cold-induced gastric emptying but
888 not brain c-Fos induction. *Peptides* 22: 81-90, 2001.
- 889 **Mason P.** Contributions of the medullary raphe and ventromedial reticular region to pain modulation and
890 other homeostatic functions. *Annu Rev Neurosci* 24: 737-777, 2001.
- 891 **Mason P.** Deconstructing endogenous pain modulations. *J Neurophysiol* 94: 1659-1663, 2005a.
- 892 **Mason P.** Ventromedial medulla: pain modulation and beyond. *J Comp Neurol* 493: 2-8, 2005b.
- 893 **Mason P.** Descending pain modulation as a component of homeostasis. In: Pain, edited by Cervero F and
894 Jensen TS. Elsevier, 2006, p. 211-218.
- 895 **Mason P.** From descending pain modulation to obesity via the medullary raphe. *Pain* 152: S20-S24, 2011.
- 896 **Mason P.** Medullary circuits for nociceptive modulation. *Curr Opin Neurobiol* 22: 640-645, 2012.
- 897 **Mason P, Floeter MK, Fields HL.** Somatodendritic morphology of on- and off-cells in the rostral
898 ventromedial medulla. *J Comp Neurol* 301: 23-43, 1990.
- 899 **McAllen RM, Tanaka M, Ootsuka Y, McKinley MJ.** Multiple thermoregulatory effectors with
900 independent central controls. *Eur J Appl Physiol* 109: 27-33, 2010.
- 901 **Meessen H, Olszewski J.** *A Cytoarchitectonic Atlas of the Rhombencephalon of the Rabbit.* Basel: Karger,
902 1949.
- 903 **Meng ID, Manning BH, Martin WJ, Fields HL.** An analgesia circuit activated by cannabinoids. *Nature*
904 395: 381-383, 1998.
- 905 **Morgan MM, Fields HL.** Pronounced changes in the activity of nociceptive modulatory neurons in the
906 rostral ventromedial medulla in response to prolonged thermal noxious stimuli. *J Neurophysiol* 72: 1161-
907 1170, 1994.
- 908 **Morrison SF.** RVLN and raphe differentially regulate sympathetic outflows to splanchnic and brown
909 adipose tissue. *Am J Physiol* 276: R962-R973, 1999.
- 910 **Morrison SF.** Differential regulation of brown adipose and splanchnic sympathetic outflows in rat: roles of
911 raphe and rostral ventrolateral medulla neurons. *Clin Exp Pharmacol Physiol* 28: 138-143, 2001.
- 912 **Morrison SF.** Raphe pallidus neurons mediate prostaglandin E₂-evoked increases in brown adipose tissue
913 thermogenesis. *Neuroscience* 121: 17-24, 2003.
- 914 **Morrison SF.** Activation of 5-HT_{1A} receptors in raphe pallidus inhibits leptin-evoked increases in brown
915 adipose tissue thermogenesis. *Am J Physiol Regul Integr Comp Physiol* 286: R832-R837, 2004.
- 916 **Morrison SF.** 2010 Carl Ludwig Distinguished Lectureship of the APS Neural Control and Autonomic
917 Regulation Section: Central neural pathways for thermoregulatory cold defense. *J Appl Physiol* 110:
918 1137-1149, 2011.
- 919 **Morrison SF, Gebber GL.** Axonal branching patterns and funicular trajectories of raphespinal
920 sympathoinhibitory neurons. *J Neurophysiol* 53: 759-772, 1985.
- 921 **Morrison SF, Sved AF, Passerin AM.** GABA-mediated inhibition of raphe pallidus neurons regulates
922 sympathetic outflow to brown adipose tissue. *Am J Physiol* 276: R290-R297, 1999.

- 923 **Morrison SF, Ramamurthy S, Young JB.** Reduced rearing temperature augments responses in sympathetic
924 outflow to brown adipose tissue. *J Neurosci* 20: 9264-9271, 2000.
- 925 **Morrison SF, Nakamura K, Madden CJ.** Central control of thermogenesis in mammals. *Exp Physiol* 93:
926 773-797, 2008.
- 927 **Morrison SF, Madden CJ, Tupone D.** Central control of brown adipose tissue thermogenesis. *Front*
928 *Endocrinol (Lausanne)* 3, article 5: 1-19, 2012.
- 929 **Myers RD.** Injection of solutions into cerebaltissue: relation between volume and diffusion. *Physiol Behav*
930 1: 171-174, 1966.
- 931 **Nagashima K, Nakai S, Tanaka M, Kanosue K.** Neuronal circuitries involved in thermoregulation. *Auton*
932 *Neurosci* 85: 18-25, 2000.
- 933 **Nakamura K.** Central circuitries for body temperature regulation and fever. *Am J Physiol Regul Integr*
934 *Comp Physiol* 301: R1207-R1228, 2011.
- 935 **Nakamura K, Morrison SF.** Central efferent pathways mediating skin cooling-evoked sympathetic
936 thermogenesis in brown adipose tissue. *Am J Physiol Regul Integr Comp Physiol* 292: R127-R136, 2007.
- 937 **Nakamura K, Morrison SF.** A thermosensory pathway that controls body temperature. *Nat Neurosci* 11:
938 62-71, 2008.
- 939 **Nakamura K, Morrison SF.** Central efferent pathways for cold-defensive and febrile shivering. *J Physiol*
940 *(Lond)* 589: 3641-3658, 2011.
- 941 **Nakamura K, Matsumura K, Hubschle T, Nakamura Y, Hioki H, Fujiyama F, Boldogkői Z, König M,**
942 **Thiel HJ, Gerstberger R, Kobayashi S, Kaneko T.** Identification of sympathetic premotor neurons in
943 medullary raphe regions mediating fever and other thermoregulatory functions. *J Neurosci* 24: 5370-
944 5380, 2004.
- 945 **Nason MWJr, Mason P.** Modulation of sympathetic and somatomotor function by the ventromedial
946 medulla. *J Neurophysiol* 92: 510-522, 2004.
- 947 **Neubert MJ, Kincaid W, Heinricher MM.** Nociceptive facilitating neurons in the rostral ventromedial
948 medulla. *Pain* 110: 158-165, 2004.
- 949 **Newman DB.** Distinguishing rat brainstem reticulospinal nuclei by their neuronal morphology. I. Medullary
950 nuclei. *J Hirnforsch* 26: 187-226, 1985.
- 951 **Nicholson SH, Suckling CJ, Iversen LL.** GABA analogues: conformational analysis of effects on
952 [3H]GABA binding to postsynaptic receptors in human cerebellum. *J Neurochem* 32: 249-252, 1979.
- 953 **Olszewski J, Baxter D.** *Cytoarchitecture of the Human Brain Stem.* Basel: Karger, 1954.
- 954 **Ootsuka Y, McAllen RM.** Interactive drives from two brain stem premotor nuclei are essential to support
955 rat tail sympathetic activity. *Am J Physiol Regul Integr Comp Physiol* 289: R1107-R1115, 2005.
- 956 **Ootsuka Y, McAllen RM.** Comparison between two rat sympathetic pathways activated in cold defense.
957 *Am J Physiol Regul Integr Comp Physiol* 291: R589-R595, 2006.
- 958 **Ootsuka Y, Blessing WW, McAllen RM.** Inhibition of rostral medullary raphe neurons prevents cold-
959 induced activity in sympathetic nerves to rat tail and rabbit ear arteries. *Neurosci Lett* 357: 58-62, 2004.
- 960 **Paxinos G, Watson C.** *The Rat Brain in Stereotaxic Coordinates.* New York: Elsevier/Academic Press,
961 2005.
- 962 **Pinedé I, Pollin B, Meert T, Plaghki L, Le Bars D.** Psychophysics of a nociceptive test in the mouse.
963 *PLoS ONE* 7: e36699, 2012.
- 964 **Potrebic SB, Mason P.** Three-dimensional analysis of the dendritic domains of on- and off-cells in the
965 rostral ventromedial medulla. *J Comp Neurol* 337: 83-93, 1993.
- 966 **Rathner JA, McAllen RM.** Differential control of sympathetic drive to the rat tail artery and kidney by
967 medullary premotor cell groups. *Brain Res* 834: 196-199, 1999.
- 968 **Rathner JA, Owens NC, McAllen RM.** Cold-activated raphe-spinal neurons in rats. *J Physiol (Lond)* 535:
969 841-854, 2001.

- 970 **Rathner JA, Madden CJ, Morrison SF.** Central pathway for spontaneous and prostaglandin E₂-evoked
971 cutaneous vasoconstriction. *Am J Physiol Regul Integr Comp Physiol* 295: R343-R354, 2008.
- 972 **Romanovsky AA.** Thermoregulation: some concepts have changed. Functional architecture of the
973 thermoregulatory system. *Am J Physiol Regul Integr Comp Physiol* 292: R37-R46, 2007.
- 974 **Romanovsky AA, Ivanov AI, Shimansky YP.** Selected contribution: ambient temperature for experiments
975 in rats: a new method for determining the zone of thermal neutrality. *J Appl Physiol* 92: 2667-2679, 2002.
- 976 **Rosland JH.** The formalin test in mice: the influence of ambient temperature. *Pain* 45: 211-216, 1991.
- 977 **Salo LM, Nalivaiko E, Anderson CR, McAllen RM.** Control of cardiac rate, contractility, and
978 atrioventricular conduction by medullary raphe neurons in anesthetized rats. *Am J Physiol Heart Circ*
979 *Physiol* 296: H318-H324, 2009.
- 980 **Smith JE, Jansen AS, Gilbey MP, Loewy AD.** CNS cell groups projecting to sympathetic outflow of tail
981 artery: neural circuits involved in heat loss in the rat. *Brain Res* 786: 153-164, 1998.
- 982 **Strack AM, Sawyer WB, Hughes JH, Platt KB, Loewy AD.** A general pattern of CNS innervation of the
983 sympathetic outflow demonstrated by transneuronal pseudorabies viral infections. *Brain Res* 491: 156-
984 162, 1989.
- 985 **Syková E, Nicholson C.** Diffusion in brain extracellular space. *Physiol Rev* 88: 1277-1340, 2008.
- 986 **Székely, M.** Skin temperature-skin blood flow: assessment of thermoregulatory changes. *Acta Physiol Hung*
987 68: 284, 1986.
- 988 **Taber E, Brodal A, Walberg F.** The raphe nuclei of the brain stem in the cat. I. Normal topography and
989 cytoarchitecture and general discussion. *J Comp Neurol* 114: 161-187, 1960.
- 990 **Tanaka M, Nagashima K, McAllen RM, Kanosue K.** Role of the medullary raphe in thermoregulatory
991 vasomotor control in rats. *J Physiol (Lond)* 540: 657-664, 2002.
- 992 **Tanaka M, Ootsuka Y, McKinley MJ, McAllen RM.** Independent vasomotor control of rat tail and
993 proximal hairy skin. *J Physiol* 582: 421-433, 2007.
- 994 **Thorington RWJr.** The biology of rodent tails: a study of form and function. *Arctic Aeromedical*
995 *Laboratory* TR-65-8: 1-138, 1966.
- 996 **Thurston CL, Helton ES.** Effects of intravenous phenylephrine on blood pressure, nociception, and neural
997 activity in the rostral ventral medulla in rats. *Brain Res* 717: 81-90, 1996.
- 998 **Thurston CL, Randich A.** Effects of vagal afferent stimulation on ON and OFF cells in the rostroventral
999 medulla: relationships to nociception and arterial blood pressure. *J Neurophysiol* 67: 180-196, 1992.
- 1000 **Thurston CL, Randich A.** Responses of on and off cells in the rostral ventral medulla to stimulation of
1001 vagal afferents and changes in mean arterial blood pressure in intact and cardiopulmonary deafferented
1002 rats. *Pain* 62: 19-38, 1995.
- 1003 **Tjølsen A, Hole K.** Animal models of analgesia. In: Pharmacology of pain, edited by Dickenson AH and
1004 Besson JM. Berlin: Springer, 1997, p. 1-20.
- 1005 **Tjølsen A, Berge O-G, Hunskaar S, Rosland JH, Hole K.** The formalin test: an evaluation of the method.
1006 *Pain* 51: 5-17, 1992.
- 1007 **Tóth IE, Tóth DE, Boldogkoi Z, Hornyák A, Palkovits M, Blessing WW.** Serotonin-synthesizing neurons
1008 in the rostral medullary raphe/parapyramidal region transneuronally labelled after injection of
1009 pseudorabies virus into the rat tail. *Neurochem Res* 31: 277-286, 2006.
- 1010 **Vanegas H, Barbaro NM, Fields HL.** Tail-flick related activity in medullospinal neurons. *Brain Res* 321:
1011 135-141, 1984.
- 1012 **Vianna DM, Allen C, Carrive P.** Cardiovascular and behavioral responses to conditioned fear after
1013 medullary raphe neuronal blockade. *Neuroscience* 153: 1344-1353, 2008.
- 1014 **Wu Y, Jiji LM, Lemons DE, Weinbaum S.** A non-uniform three-dimensional perfusion model of rat tail
1015 heat transfer. *Phys Med Biol* 40: 789-806, 1995.

- 1016 **Xu M, Kim CJ, Neubert MJ, Heinricher MM.** NMDA receptor-mediated activation of medullary pro-
1017 nociceptive neurons is required for secondary thermal hyperalgesia. *Pain* 127: 253-262, 2007.
- 1018 **Yoshida K, Nakamura K, Matsumura K, Kanosue K, König M, Thiel HJ, Boldogkői Z, Toth I, Roth J,**
1019 **Gerstberger R, Hübschle T.** Neurons of the rat preoptic area and the raphe pallidus nucleus innervating
1020 the brown adipose tissue express the prostaglandin E receptor subtype EP3. *Eur J Neurosci* 18: 1848-
1021 1860, 2003.
- 1022 **Young AA, Dawson NJ.** Evidence for on-off control of heat dissipation from the tail of the rat. *Can J*
1023 *Physiol Pharmacol* 60: 392-398, 1982.
- 1024 **Zaretsky DV, Zaretskaia MV, DiMicco JA.** Stimulation and blockade of GABA(A) receptors in the raphe
1025 pallidus: effects on body temperature, heart rate, and blood pressure in conscious rats. *Am J Physiol Regul*
1026 *Integr Comp Physiol* 285: R110-R116, 2003a.
- 1027 **Zaretsky DV, Zaretskaia MV, Samuels BC, Cluxton LK., DiMicco JA.** Microinjection of muscimol into
1028 raphe pallidus suppresses tachycardia associated with air stress in conscious rats. *J Physiol* 546: 243-250,
1029 2003b.
- 1030 **Zimmermann M.** Ethical guidelines for investigations of experimental pain in conscious animals. *Pain* 16:
1031 109-110, 1983.
- 1032

1033 **FIGURE LEGENDS**

1034

1035 **Figure 1.** Procedure to analyze the muscimol-induced variations of skin temperature. **A & B.** Abscissa: time
 1036 in min with reference to the end of the microinjection. Ordinate: temperature in °C. The grey area
 1037 corresponds to the time intervals < 7.5 min and 7.5-15 min post-injection, delimited by vertical dotted lines.

1038 **A.** Analysis of temperature variations observed from an ipsilateral hind-paw ($T_{\text{paw-ipsi}}$). The thin yellow line is
 1039 the temporal evolution of the temperature recorded during the 5-min control period and the following 30-min
 1040 post-injection. The thick yellow line is the corresponding adjusted sigmoid Boltzmann curve $T_{\text{adj}} = T_{\text{min}} +$
 1041 $\Delta T_{\text{skin}} / \{1 + \exp[-(t - t_x)/s]\}$, with $R^2 = 0.99$ (equation in the upper left corner of the graph). The adjusted
 1042 parameters of the function are shown in red, namely the adjusted skin temperature during the control period
 1043 ($T_{\text{min}} = 24.2^\circ\text{C}$), the adjusted maximal skin temperature at the end of the process ($T_{\text{max}} = 32.4^\circ\text{C}$), the
 1044 amplitude of skin temperature variation ($\Delta T_{\text{skin}} = T_{\text{max}} - T_{\text{min}} = 8.2^\circ\text{C}$), the inflection point (t_x , $T_x = T_{\text{min}} +$
 1045 $\Delta T_{\text{skin}}/2$) [(8.8 min, 28.3°C)] of the sigmoid represented by a red point. The beginning (t_{min}) and end (t_{max}) of
 1046 the ascending phase of vasodilatation were then calculated by considering the 10 and 90% percentiles of
 1047 ΔT_{skin} : $t_{\text{min}} = t_x - \text{Ln}(1/0.1-1) \cdot s^{-1} = 4.9$ min and $t_{\text{max}} = t_x - \text{Ln}(1/0.9-1) \cdot s^{-1} = 13.9$ min, represented by white
 1048 points. **B.** Calculation of the beginning of the ascending phase of vasodilatation observed from the
 1049 corresponding three other recorded zones ($T_{\text{paw-contra}}$, $T_{\text{tail-prox}}$, $T_{\text{tail-dist}}$). The thin and thick curves represent the
 1050 genuine and adjusted curves, respectively. The green, dark blue and light blue curves correspond to the
 1051 contralateral hind-paw, proximal and distal parts of the tail, respectively (corresponding equations provided
 1052 in the upper left hand corner of the graph). Calculations of t_{min} were made as in A, except for the proximal
 1053 part of the tail for which a 15% percentile was used in place of the 10% (see text). **C.** Histogram showing the
 1054 distribution of the beginning of the ascending phase of vasodilatation (t_{min}) for the ipsilateral hind-paws,
 1055 allowing the categorization into three groups: group 1: **$t_{\text{min}} < 7.5$ min**; group 2: **$7.5 < t_{\text{min}} < 15$ min**; group 3:
 1056 **$t_{\text{min}} > 15$ min.**

1057

1058

1059 **Figure 2.** Example of effects elicited by muscimol microinjection in the RVM. **A.** Example of pictures taken
 1060 at 0, 5, 10, 15, 20, 25, 30 min post-injection of a thermographic movie recorded with a 320*240 pixels
 1061 resolution (See the corresponding Supporting video S1). The false colors scale of temperature is shown in
 1062 the right hand part of the picture. **B.** Temporal evolution of the temperatures recorded during the 5-min
 1063 control and 30-min post-injection periods. Abscissa: time in min. Ordinate: temperature in °C. The eight
 1064 analyzed zones (10 pixels each) are indicated on the drawing in the right hand part of the figure. $T_{\text{paw-ipsi}}$
 1065 (yellow) and $T_{\text{paw-contra}}$ (green) corresponds to the skin temperature of the ipsi- and contralateral hind-paw,
 1066 respectively. $T_{\text{tail-prox}}$ (dark blue) and $T_{\text{tail-dist}}$ (light blue) corresponds to the skin temperatures of the proximal
 1067 and distal part of the tail, respectively; there are three additional intermediate blue sites between these two
 1068 sites. T_{amb} (brown) corresponds to the ambient temperature measured from a small piece of wood. Note the
 1069 stability of the control period in vasoconstriction with skin temperatures near T_{amb} . Following the
 1070 microinjection, the ipsilateral hind-paw skin temperature raised first, followed by the proximal and distal
 1071 parts of the tail and at last the contralateral hind-paw. **C.** Temporal evolution of core temperature (T_{core}).
 1072 Abscissa: time in min. Ordinate: temperature in °C. Note the decrease in core temperature, starting shortly
 1073 after the rise of $T_{\text{paw-ipsi}}$. **D.** Corresponding Heat loss Index [$\text{HLI} = (T_{\text{skin}} - T_{\text{amb}})/(T_{\text{core}} - T_{\text{amb}})$ (Romanovsky et
 1074 al. 2002)] for the seven skin areas considered. **E.** Temporal evolution of MAP. Abscissa: time in min.
 1075 Ordinate: MAP in mmHg. Note the slight transitory increase in MAP shortly after the microinjection,
 1076 followed by a sustained drop and then a progressive stabilization after 8-min post-injection. **F.** Temporal
 1077 evolution of HR. Abscissa: time in min. Ordinate: HR in beat per minute (bpm). Note the slight transitory
 1078 increase in HR shortly after the microinjection, followed by a sustained drop and then a progressive
 1079 stabilization after 9-min post-injection. **G.** Temporal evolution of ETCO_2 . Abscissa: time in min. Ordinate:
 1080 ETCO_2 in %. Note the parallel changes in E, F and G. **H.** Localization of the site of injection drawn on a
 1081 frontal section of the brain in plane -2.3 mm caudal to the inter-aural line. The center of the injection site is
 1082 located 0.3 mm lateral to the midline and 0.4 mm below the inter-aural line. Abbreviations: 7: facial nucleus,
 1083 GiA: gigantocellular reticular nucleus pars alpha; ml: medial lemniscus; PPy: parapyramidal nucleus; py:
 1084 pyramidal tract; RMg: raphe magnus nucleus; RPa: raphe pallidus nucleus.

1085

1086

1087 **Figure 3.** Temporal evolution of the skin temperature recorded from the hind-paws, following muscimol
1088 microinjections. Abscissa: time in min, Ordinate: temperature variation in °C (mean \pm 95% confidence
1089 interval). As indicated in the left hand lower corner, yellow and green curves are data adjusted to a
1090 Boltzmann sigmoid (see Fig. 1) from the ipsi- ($T_{\text{paw-ipsi}}$) and contralateral ($T_{\text{paw-contra}}$) hind-paw skin
1091 temperature, respectively. The experiments were divided in three groups on the basis of the distribution of
1092 the beginning (t_{min}) of the ascending phase of vasodilatation from the ipsilateral hind-paw. **A.** Group 1: $t_{\text{min}} <$
1093 7.5 min). **B.** Group 2: $7.5 < t_{\text{min}} < 15$ min. **C.** Group 3: $t_{\text{min}} > 15$ min. See text and table 1A.
1094

1095 **Figure 4.** Overall effects elicited by muscimol microinjection on the skin temperature recorded from the
1096 hind-paws. **A.** contralateral hind-paw; **B.** ipsilateral hind-paw. Schema of frontal sections of the brain from
1097 inter-aural $z = -0.8$ (top) to $z = -3.3$ mm (bottom), adapted from Paxinos and Watson (2005). The circles
1098 indicate the center of the corresponding injection sites, with a diameter scaled to a 50 nl sphere. The black
1099 symbols represent the early latency group with an onset of vasodilatation in less than 7.5 min. The grey
1100 symbols correspond to the intermediate latency group with an onset of vasodilatation between 7.5 and 15
1101 min. The white symbols stand for the group that included the experiments with an onset of vasodilatation in
1102 more than 15-min (or did not react at all). Abbreviations: 7: facial nucleus; GiA: gigantocellular reticular
1103 nucleus pars alpha; ml: medial lemniscus; PPy: parapyramidal nucleus; py: pyramidal tract; RMg: raphe
1104 magnus nucleus; RPa: raphe pallidus nucleus.
1105

1106 **Figure 5.** Three-dimensional mapping of the hind-paw response latencies t_{\min} as a function of injection sites.
1107 The responses obtained from the left and right paw were merged, by expressing the location of the injection
1108 site as ipsilateral (positive x-axis) vs. contralateral (negative x-axis) relative to the paw. On the left graphs,
1109 the interpolated response latencies are indicated by the false colors (scale shown in the lower right hand part
1110 of the figure). They are adjusted on frontal sections of the brain from inter-aural $z = -0.8$ (top) to $z = -3.3$ mm
1111 (bottom) with y being the ventro-dorsal coordinate, again with reference to the interaural line. The right
1112 drawings are adapted from Paxinos and Watson (2005). Abbreviations: 7: facial nucleus; GiA:
1113 gigantocellular reticular nucleus pars alpha; LPGi: lateral paragigantocellular nucleus; ml: medial lemniscus;
1114 PPy: parapyramidal nucleus; py: pyramidal tract; RMg: raphe magnus nucleus; RPa: raphe pallidus nucleus.
1115
1116

1117 **Figure 6.** Temporal evolution of the skin temperature recorded from the tail, following muscimol
1118 microinjections. Abscissa: time in min, Ordinate: temperature variation in °C (mean \pm 95% confidence
1119 interval). As indicated in the left hand lower corner, dark blue and blue colors are data adjusted to a
1120 Boltzmann sigmoid (see Fig. 1) from the skin temperature of the proximal ($T_{\text{tail-prox}}$) and distal ($T_{\text{tail-dist}}$) part
1121 of the tail, respectively. The experiments were divided in three groups on the basis of the distribution of the
1122 beginning (t_{min}) of the ascending phase of vasodilatation on the distal part of the tail. **A.** Group 1: $t_{\text{min}} < 7.5$
1123 min). **B.** Group 2: $7.5 < t_{\text{min}} < 15$ min. **C.** Group 3: $t_{\text{min}} > 15$ min. See text and table 1B.
1124

1125 **Figure 7.** Overall effects elicited by muscimol microinjection on the skin temperature recorded from the tail.
1126 **A.** proximal part of the tail; **B.** distal part of the tail. Symbols and abbreviations as in figure 4.
1127
1128
1129

1130 **Figure 8.** Three-dimensional mapping of the tail response latencies t_{\min} as a function of injection sites. **A.**
1131 proximal part of the tail. **B.** distal part of the tail. The interpolated response latencies are indicated by the
1132 false colors (scale shown in the bottom of the figure). They are adjusted on frontal sections of the brain from
1133 inter-aural $z = -0.8$ (top) to $z = -3.3$ mm (bottom) with x and y being the lateral and ventro-dorsal coordinate,
1134 respectively, again with reference to the interaural line. Symbols and abbreviations as in figure 5.
1135

1136 **Figure 9. A.** Schema of frontal sections of the brain from inter-aural -0.8 (top) to -3.3 mm (bottom), adapted
1137 from Paxinos and Watson (2005). Symbols and abbreviations as in figure 4. The data were synthesized by
1138 regrouping the experiments in three new groups, again on the basis of the beginning time t_{\min} of the
1139 ascending phase of vasodilatation, considering all skin areas either on the tail or the paws. The black
1140 symbols represent the early latency group with $t_{\min} < 15 \text{ min}$ for all considered skin areas either on the tail
1141 or the paws. The grey symbols correspond to the intermediate latency group with $t_{\min} < 15 \text{ min}$ for at least
1142 **one** of these areas. The white symbols correspond to the late latency group with $t_{\min} > 15 \text{ min}$ for all
1143 considered skin areas. **B.** Variation of skin temperature ($\Delta^{\circ}\text{C}$) recorded from the ipsilateral hind-paw. **C.**
1144 Variation of skin temperature ($\Delta^{\circ}\text{C}$) recorded from the contralateral hind-paw. **D.** Variation of skin
1145 temperature ($\Delta^{\circ}\text{C}$) recorded from the distal part of the tail. **E.** Variation of skin temperature ($\Delta^{\circ}\text{C}$) recorded
1146 from the proximal part of the tail. **F.** Variation of core temperature ($\Delta^{\circ}\text{C}$). In the 1st group, T_{core} declined
1147 linearly as early as the first minute post-injection); for the 2nd group, T_{core} decline is parallel to the 1st's but
1148 with 15-min delay and the 3rd group's T_{core} remained stable. **G.** Variation of mean arterial blood pressure
1149 (ΔmmHg). Note a slight transitory increase of MAP in all groups, shortly after the microinjection followed
1150 by a sustained drop. This was followed by a slow decline in the first group, stabilization in the 3rd group
1151 blood, while the 2nd group spread out in-between. **H.** Corresponding variations of heart rate (Δbpm). **I.**
1152 Variation of end-tidal CO_2 ($\Delta\%$). The corresponding numerical data are provided in table 3.
1153

1154

1155 **Figure 10.** We proposed and verified experimentally a simple model for computing the TFL in the rat,
1156 taking into account the power of the radiant heat source, the initial temperature of the skin, the core
1157 temperature or the site of stimulation on the tail (Benoist et al. 2008). This model is used here to compute the
1158 predictable variations of the TFL introduced by muscimol in the positive cases of the present experiments.
1159 Since the decisional and motor latencies were estimated 134 and 4 ms, respectively (Benoist et al. 2008) and
1160 considering a site of stimulation on the mid-tail far-off the dorsal horn entry zone by 200 mm, the model
1161 provides the following equation giving the tail-flick latency: $TFL (s) = [(36.8 - 0.73 \cdot T_{\text{mid-tail}})^2 / \alpha +$
1162 $90 / (0.041 \cdot T_{\text{core}} - 0.47) + 110 / (0.041 \cdot T_{\text{mid-tail}} - 0.47) + 138] / 1000$ where α is the slope of the squared
1163 temperature variation, witness of the power of the radiant heat source. Experimental data are from the
1164 experiments where the beginning of the ascending phase of vasodilatation was < 15 min either on the tail or
1165 the paws (Black group in figure 9); they include both the mean temperatures of the core (T_{core} , brown line)
1166 and the middle of the tail ($T_{\text{mid-tail}}$, blue line). In the control situation, the model provides tail-flick latencies
1167 (red lines) in the 3-4 seconds range for α in the 0.08-0.2°C²/s range: the model foretells a 30-35% decrease
1168 of the TFL following muscimol microinjections in the sites indicated by a black circle in Fig. 9A.

1169

1170 **Supporting Video.** Thermographic recording at 1 Hz with a 320x240 pixels resolution, compressed and
1171 presented in 14 seconds, made during the 5-min control and 30-min post-injection periods. The
1172 thermography is presented in false colors (scale in the left). The graph is the corresponding temporal
1173 evolution of the skin temperature recorded on 5 points distributed from the base to the tip of the tail (blue
1174 points) and the right (yellow point) and left (green point) hind-paws as indicated on the right hand picture.
1175 The ambient temperature was measured on an inert piece of wood (brown point). The localization of the site
1176 of injection of muscimol (50 nmol, 50 nl) is drawn on a frontal section of the brain in plane -2.3 mm caudal
1177 to the inter-aural line. Abbreviations: Gi: gigantocellular reticular nucleus; GiA: gigantocellular reticular
1178 nucleus pars alpha; ml: medial lemniscus; RMg: raphe magnus nucleus; RPa: raphe pallidus nucleus; py:
1179 pyramidal tract.
1180

1181 A: paws (see Fig. 3)

		T_{\min} (°C)	ΔT_{skin} (°C)	t_{\min} (min)	t_x (min)	Δt (min)	$\Delta T_{\text{skin}}/\Delta t$ (°C/min)
ipsilateral	group 1	25.4 (25.2-25.7)	7.4 (7.2-7.7)	3.6 (3.4-3.8)	6.6 (7.4-5.8)	6.6 (7.4-5.8)	1.2 (1.0-1.6)
	group 2	25.4 (25.2-25.7)	7.7 (7.4-8.0)	11.3 (11.2-11.5)	15.3 (16.0-14.6)	7.9 (6.7-9.0)	7.9 (6.7-9.0)
contralateral	group 1	25.6 (25.5-25.8)	7.2 (7.0-7.4)	14.6* (12.8-16.3)	18.0* (15.8-20.2)	6.8 (5.9-7.7)	1.1 (0.9-1.3)
	group 2	25.4 (25.3-25.6)	7.9 (7.6-8.2)	23.5* (22.0-25.0)	27.8* (29.6-25.9)	8.5 (7.8-9.2)	0.9 (0.8-1.0)

1182 * P < 0.01 with respect to the corresponding value of the ipsilateral paw.

1183 B: tail (see Fig. 6)

		T_{\min} (°C)	ΔT_{skin} (°C)	t_{\min} (min)	t_x (min)	Δt (min)	$\Delta T_{\text{skin}}/\Delta t$ (°C/min)
proximal	group 1	27.7 (27.4-28.0)	4.4* (4.1-4.7)	2.4* (2.4-2.5)	8.1 (8.9-7.2)	14.2* (11.9-16.5)	0.3* (0.2-0.4)
	group 2	27.7 (27.3-28.2)	4.4* (4.0-4.9)	8.2* (8.1-8.4)	16.1 (16.9-15.3)	15.7* (13.7-17.7)	0.3* (0.2-0.4)
distal	group 1	25.2 (25.0-25.5)	5.6* (5.2-6.0)	2.4* (2.0-2.8)	8.6* (7.1-10.2)	14.7* (11.2-18.2)	0.4* (0.3-0.5)
	group 2	25.4 (25.0-25.8)	6.2* (5.7-6.7)	11.2 (11.0-11.4)	17.5* (18.6-16.4)	12.5* (10.7-14.4)	0.5* (0.4-0.6)

1184 * P < 0.05 with respect to the corresponding value of the ipsilateral paw.

1185

1186

1187 **Table 1 (see Fig. 3 and 6).** Results (expressed as means \pm confident interval 95 %) obtained following
 1188 Boltzmann sigmoid regression of individual curves of skin temperature following microinjections of
 1189 muscimol (see Fig. 1). For both the paws (A) and the tail (B), the experiments were divided in three groups
 1190 on the basis of the beginning time t_{\min} of the ascending phase of vasodilatation. Group 1: t_{\min} < **15 min for**
 1191 **all skin areas**; Group 2: t_{\min} < **15 min for at least one** skin area; Group 3 (not shown): t_{\min} > **15 min for all**
 1192 skin areas (see Fig. 3 and 6). Keys: t_x = abscissa of the inflection point of the sigmoid, Δt = duration of the
 1193 ascending phase of vasodilatation, T_{\min} = adjusted skin temperature during the control period, ΔT_{skin} =
 1194 amplitude of skin temperature variation. $\Delta T_{\text{skin}}/\Delta t$ = speed of warming. The regression coefficients R^2 of the
 1195 adjusted curves were always highly significant (> 0.98).

1195

	(A) HLI during vasoconstriction			(B) HLI during vasodilation		
	(a) control period (present study)	(b) vasoconstriction periods (El Bitar et al. 2014a)	P	(a) 30 min following muscimol	(b) vasodilation periods (El Bitar et al. 2014a)	P
T _{paw-ipsi}	0.10 (0.10-0.11)	0.13 (0.09-0.16)	0.12	0.69 (0.65-0.74)	0.92 (0.85-0.98)	< 0.00001
T _{tail-prox}	0.24 (0.22-0.25)	0.23 (0.21-0.26)	0.64	0.62 (0.57-0.67)	0.77 (0.72-0.83)	< 0.0001
T _{tail-dist}	0.04 (0.04-0.04)	0.03 (0.01-0.05)	0.06	0.55 (0.46-0.63)	0.74 (0.69-0.80)	< 0.0001

1196

1197 **Table 2.** Summary of skin vasomotor tone expressed in terms of Heat Loss Index [$HLI = (T_{skin} - T_{amb}) / (T_{core} -$
1198 $T_{amb})$] (Gordon et al. 2002; Romanovsky et al. 2002; Székely 1986), represented as means and their 95%
1199 confidence interval. Results obtained from current study (a) are compared to a previous study (b) in the
1200 extreme vasomotor tone status, namely vasoconstriction (A) and vasodilation (B). During vasoconstriction,
1201 there were no significant statistical differences between HLI observed in the two studies. By contrast, the
1202 HLI for both hind-paws and following muscimol microinjections were significantly lower than the HLI seen
1203 during the physiological vasodilation elicited during thermo-neutrality (El Bitar et al. 2014a).

1204

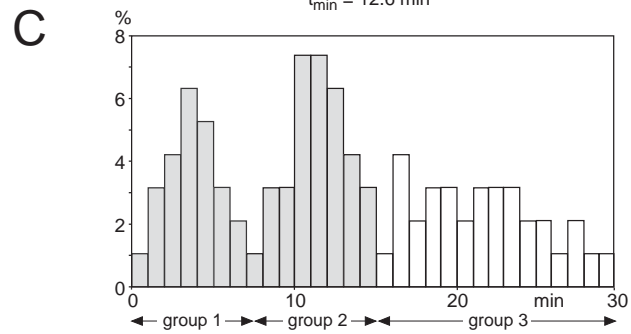
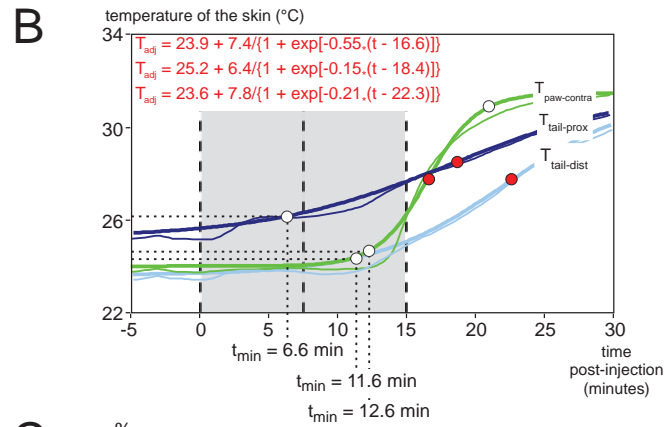
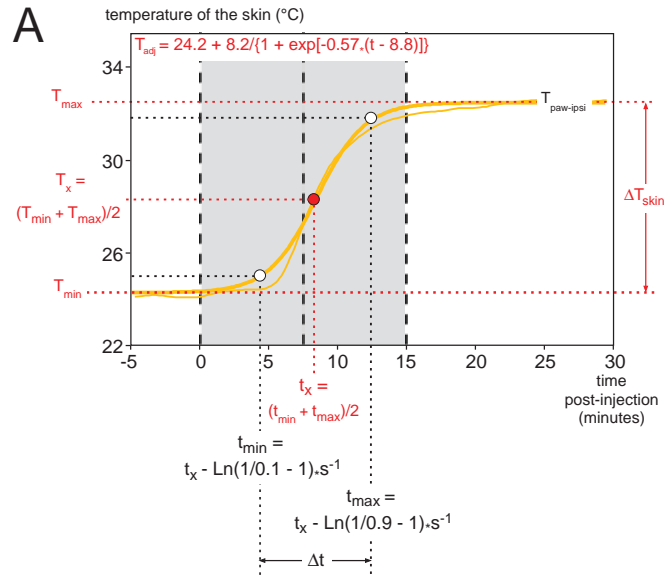
	Skin area	T _{min} (°C)	ΔT _{skin} (°C)	t _{min} (min)	t _x (min)	Δt (min)	ΔT _{skin} /Δt (°C/min)	ΔT _{core} (°C)	ΔMAP (mmHg)	ΔHR (bpm)	ΔETCO ₂ (%)
Group 1	ipsilateral paw	26.1 (25.7-26.4)	7.3 (6.9-7.6)	5.8 (5.4-6.2)	8.8 (7.8-9.8)	5.9 (4.6-7.1)	1.2 (1.0-1.7)	0.96 (0.85-1.06)	23.9 (20.1-27.7)	39 (31-48)	0.5 (0.4-0.5)
	contralateral paw	25.9 (25.7-26.1)	6.9 (6.2-6.6)	9.6 (8.7-10.4)	13.0 (11.6-14.2)	6.7 (5.7-7.6)	1.0 (0.8-1.2)				
	proximal tail	27.8 (27.4-28.1)	4.2 (3.9-4.5)	5.3 (5.0-5.6)	10.9 (9.8-11.9)	14.2 (12.4-16.0)	0.3 (0.2-0.4)				
	distal tail	25.3 (25.0-25.5)	5.6 (5.2-5.9)	5.1 (2.4-7.7)	11.7 (10.3-13.1)	13.2 (10.8-15.6)	0.4 (0.3-0.5)				
Group 2	ipsilateral paw	25.2 (25.0-25.3)	7.7 (7.5-8.0)	10.9** (10.4-11.3)	14.8** (13.9-15.8)	7.8 (6.9-8.8)	1.0 (0.9-1.1)	0.52** (0.37-0.67)	19.4* (12.5-26.3)	40 (34-45)	0.4 (0.4-0.5)
	contralateral paw	25.4 (25.2-25.5)	7.2 (7.1-7.4)	27.6** (26.5-28.6)	31.5** (32.8-30.)	7.2 (7.1-7.4)	1.0 (1.0-1.0)				
	proximal tail	25.6 (25.2-25.9)	6.0 (5.7-6.4)	10.2** (10.1-10.3)	24.8** (23.7-26.9)	29.2 (27.2-31.2)	0.2 (0.2-0.2)				
	distal tail	24.6 (24.4-24.8)	6.4 (6.2-6.6)	21.4** (22.0-20.8)	29.1** (28.0-30.3)	15.5 (14.4-16.5)	0.4 (0.4-0.5)				

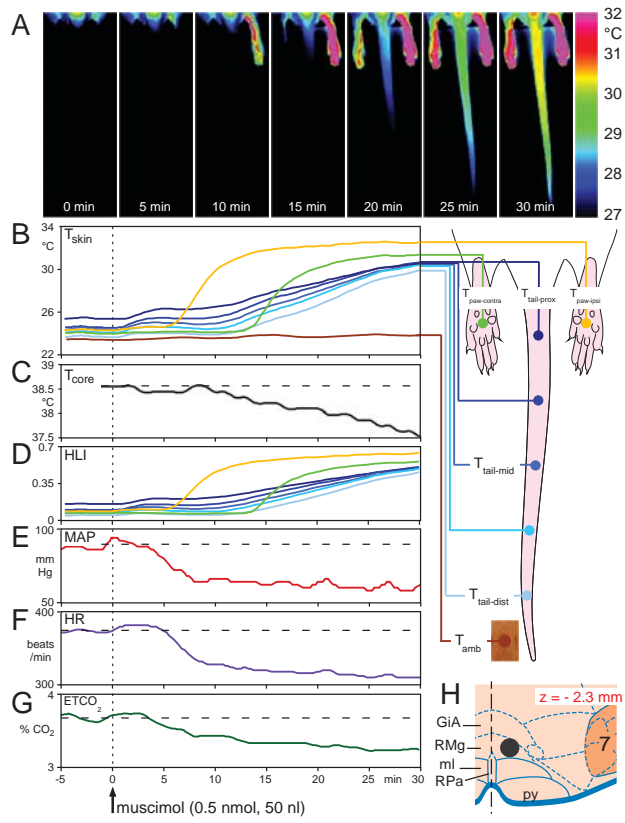
1205 * P < 0.05 ** , P < 0.01 with respect to the corresponding value in group 1.

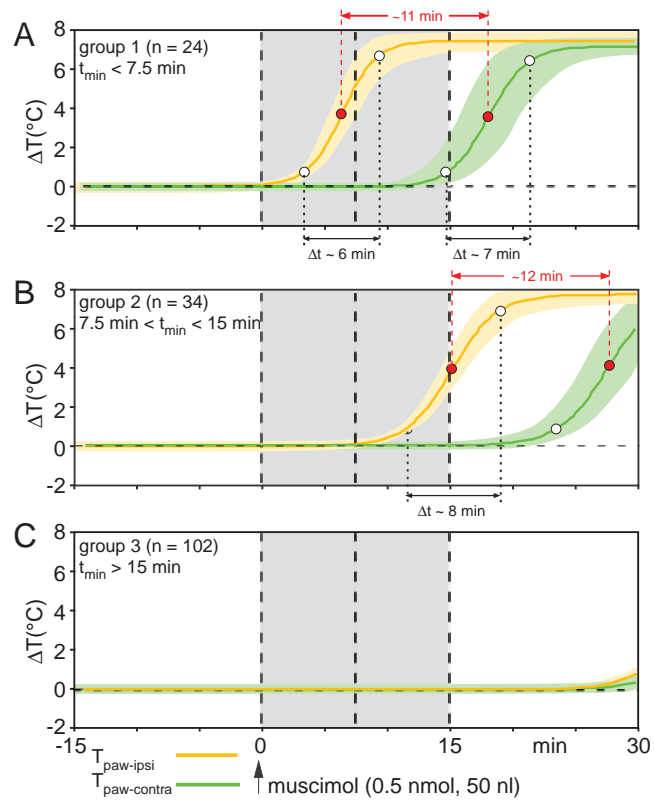
1206

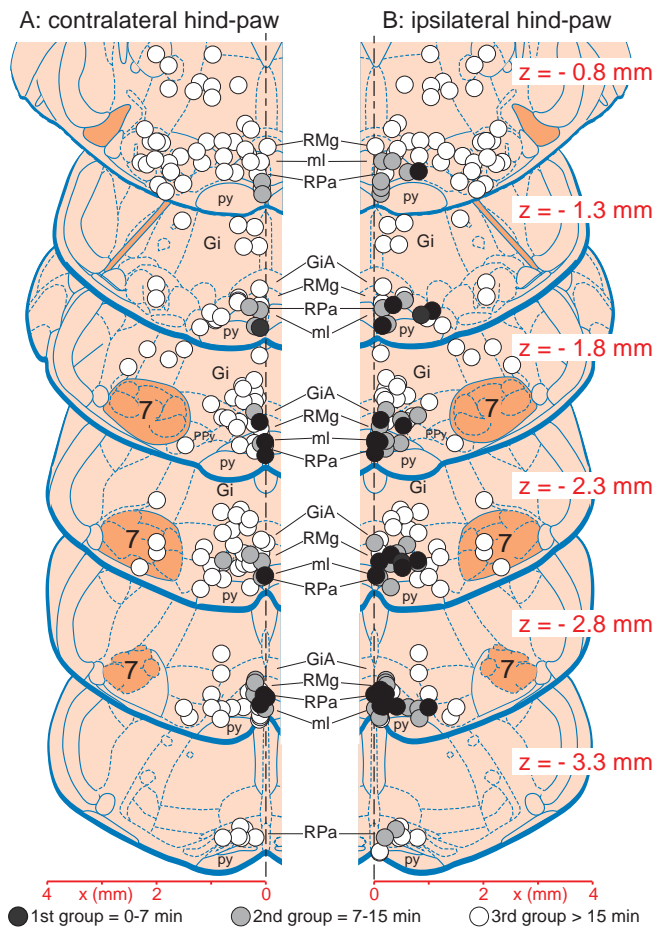
1207 **Table 3 (see Fig. 9).** Results (means ± confident interval 95%) expressed in terms of difference to mean
1208 value recorded during the control period. (1) The data represented in the five left hand columns were
1209 obtained following Boltzmann sigmoid regression of individual curves of skin temperature following
1210 microinjections of muscimol (see Fig. 1). The experiments were divided in three groups on the basis of the
1211 beginning time t_{min} of the ascending phase of vasodilatation. Group 1: t_{min} < 15 min for all skin areas; Group
1212 2: t_{min} < 15 min for at least one skin area; Group 3 (not shown): t_{min} > 15 min for all skin areas (see Fig.
1213 9B-9E). Keys: T_{min} = adjusted skin temperature during the control period, ΔT_{skin} = amplitude of skin
1214 temperature variation, t_x = abscissa of the inflection point of the sigmoid, Δt = duration of the ascending
1215 phase of vasodilatation. The regression coefficients R² of the adjusted curves were always highly significant
1216 (> 0.98). (2) The data represented in the four right hand columns are the corresponding data related to the
1217 vital signs (T_{core}, MAP, HR and ETCO₂) recorded 30 minutes following the microinjection of muscimol (see
1218 Fig. 9F-9I). The mean values for T_{core}, MAP, HR and ETCO₂ during the control period were 37.7 (37.6 -
1219 37.8)°C, 83 (77-90) mmHg, 320 (309-332) bpm, 3.65 (3.57-3.73)%, respectively. There was no statistical
1220 difference among the three groups concerning T_{core}, MAP, HR and ETCO₂ during the control period (P =
1221 0.78, 0.25, 0.77 and 0.63, respectively).

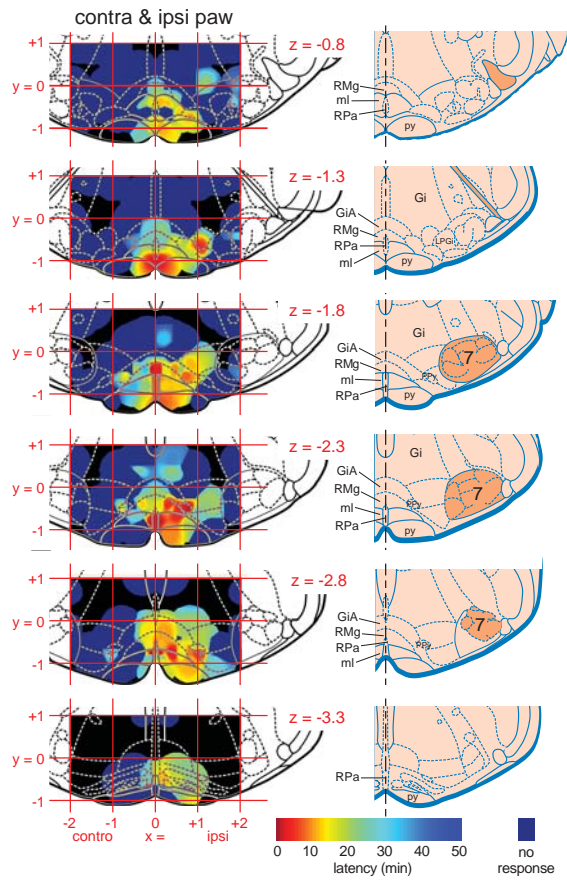
1222

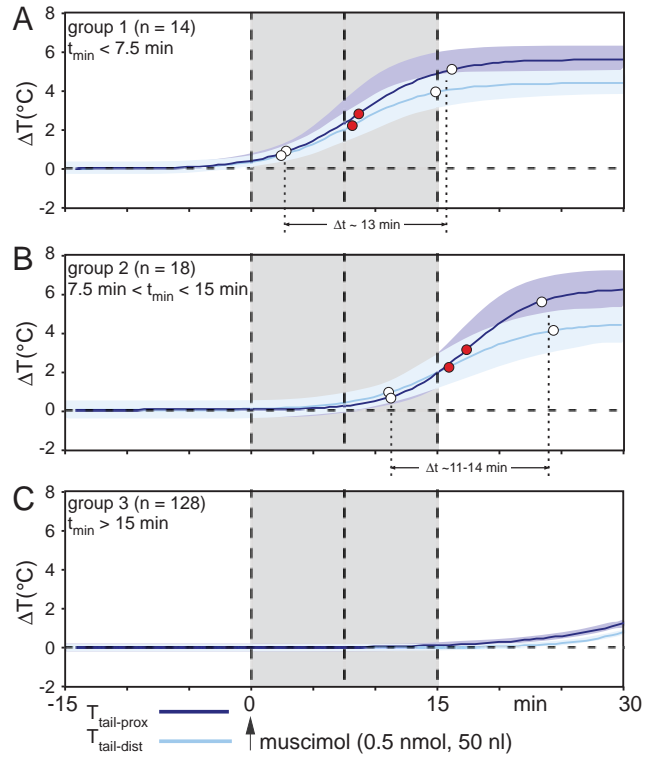


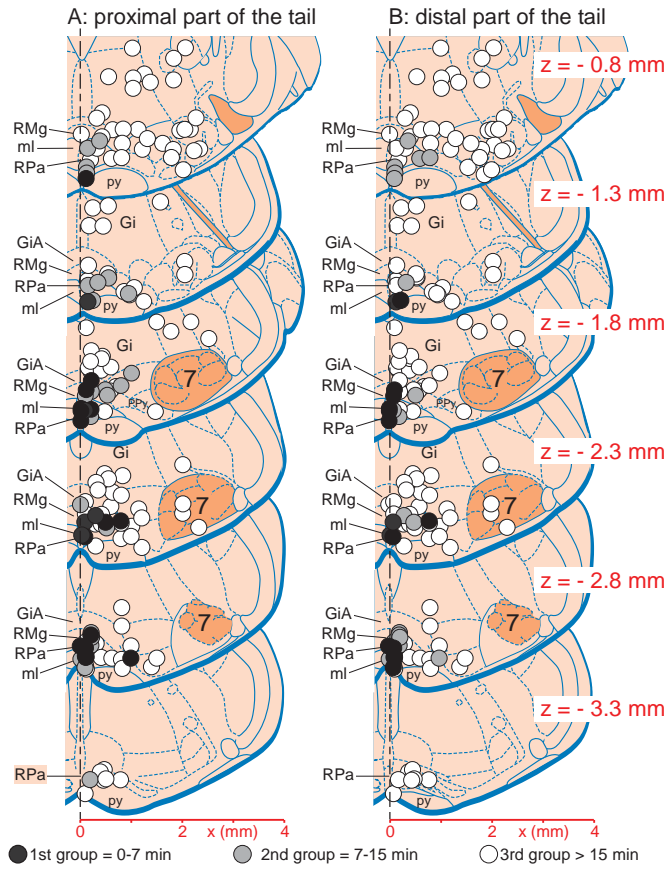


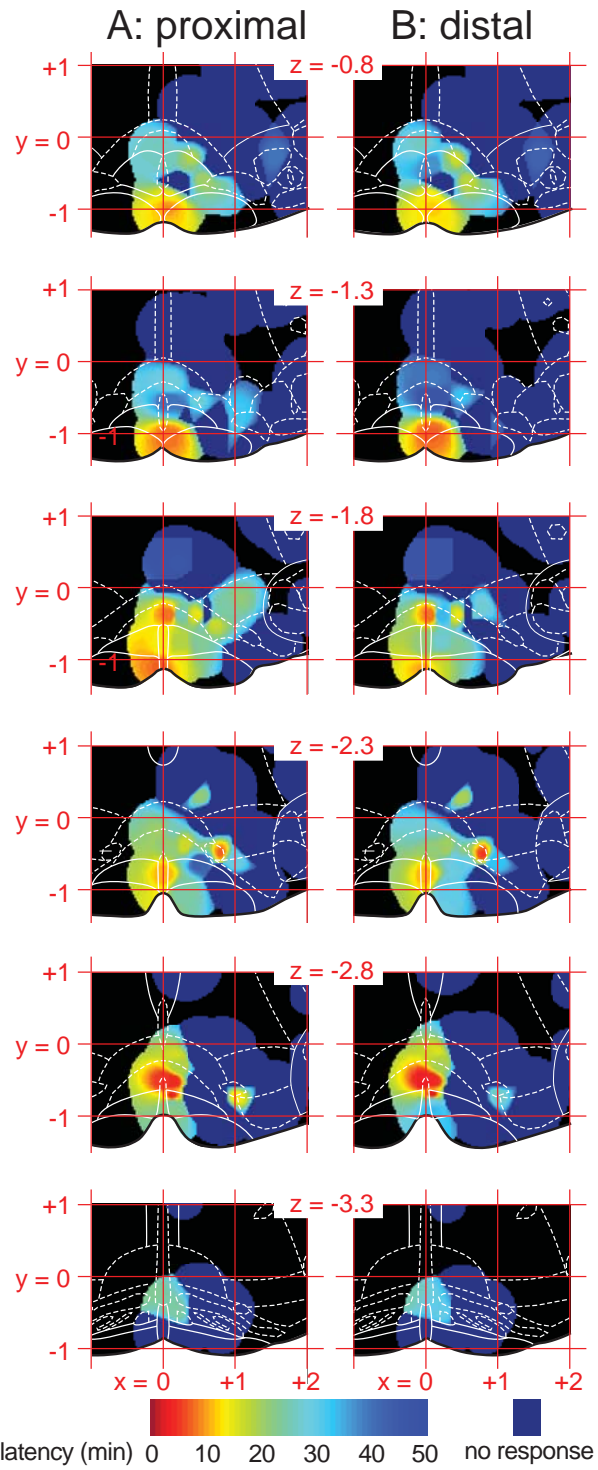


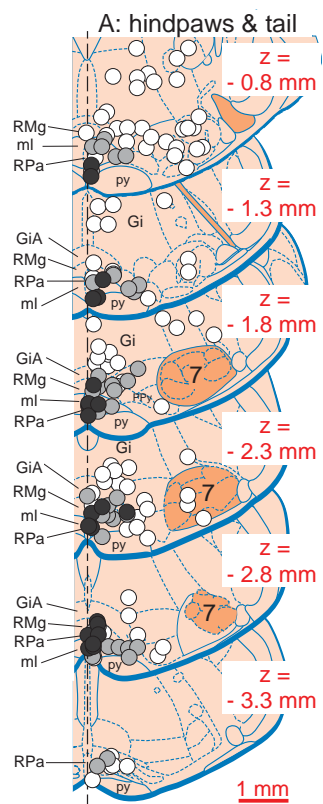












- all paws AND tail < 15 min (n = 23)
- one paw OR tail < 15 min (n = 41)
- all paws AND tail > 15 min (n = 96)

